JAMES | Journal of Advances in Modeling Earth Systems®

RESEARCH ARTICLE
10.1029/2023MS003861

New Features and Enhancements in Community Land Model (CLM5) Snow Albedo Modeling: Description, Sensitivity, and Evaluation

Cenlin He[1], Mark Flanner[2], David M. Lawrence[1], and Yu Gu[3]

[1]NSF National Center for Atmospheric Research (NCAR), Boulder, CO, USA, [2]University of Michigan Ann Arbor, Ann Arbor, MI, USA, [3]University of California Los Angeles (UCLA), Los Angeles, CA, USA

Key Points:

- We enhance CLM5 snow albedo modeling by including more realistic and physical representations of snow-aerosol-radiation interactions
- The new adding-doubling solver, nonspherical snow grains, aerosol-snow internal mixing, and updated aerosol optics show strong impacts
- The enhanced snow albedo representation improves the CLM simulated snowpack evolution and land surface conditions in many global regions

Supporting Information:

Supporting Information may be found in the online version of this article.

Correspondence to:

C. He,
cenlinhe@ucar.edu

Citation:

He, C., Flanner, M., Lawrence, D. M., & Gu, Y. (2024). New features and enhancements in community land model (CLM5) snow albedo modeling: Description, sensitivity, and evaluation. *Journal of Advances in Modeling Earth Systems*, *16*, e2023MS003861. https://doi.org/10.1029/2023MS003861

Received 6 JUN 2023
Accepted 17 JAN 2024

Abstract We enhance the Community Land Model (CLM) snow albedo modeling by implementing several new features with more realistic and physical representations of snow-aerosol-radiation interactions. Specifically, we incorporate the following model enhancements: (a) updating ice and aerosol optical properties with more realistic and accurate data sets, (b) adding multiple dust types, (c) adding multiple surface downward solar spectra to account for different atmospheric conditions, (d) incorporating a more accurate adding-doubling radiative transfer solver, (e) adding nonspherical snow grain representations, (f) adding black carbon-snow and dust-snow internal mixing representations, and (g) adding a hyperspectral (480-band vs. the default 5-band) modeling capability. These model features/enhancements are included as new CLM physics/namelist options, which allows for quantification of model sensitivity to snow albedo processes and for multi-physics model ensemble analyses for uncertainty assessment. The model updates have been included in the latest released CLM version. Sensitivity analyses reveal strong impacts of using the new adding-doubling solver, nonspherical snow grains, aerosol-snow internal mixing, updated aerosol optics, and different dust types. These enhanced snow albedo representations improve the CLM simulated global snowpack evolution and land surface conditions, with reduced biases in simulated snow surface albedo, snow cover, snow water equivalent, snow depth, and surface (2-m) air temperature over many mid-latitude mountainous regions and seasonal snowpacks but degraded performance in some northern high-latitude regions.

Plain Language Summary Snow albedo plays a critical role in the Earth system, affecting land surface energy and water balance and also serving as an important land process that feeds back to the atmosphere. Several recent studies have identified new or improved physical representations of snow albedo processes. In this study, we leverage recent advances in snow albedo modeling to implement a number of relevant new features into the widely used Community Land Model (CLM), which is the land component of the Community Earth System Model (CESM). Specifically, we improve the ice and aerosol optical properties, the treatment of dust types and downward sunlight energy distribution at different wavelength bands, the albedo computation algorithm, and the representations of snow grain shape and how aerosol is mixed with snow grains. These model updates have been included in the latest released CLM version. Overall, the enhanced snow albedo representations improve the simulated snowpack evolution and related land surface conditions in many parts of the globe.

1. Introduction

Snow albedo plays a key role in altering surface energy and water balance in the Earth system. It affects not only the evolution of snowpack states (e.g., snow depth, snow water equivalent (SWE), and snow cover) and hydrology (e.g., runoff/streamflow, reservoir storage, and flooding/drought) but also the atmosphere (e.g., surface temperature, humidity, local/regional boundary layer height, and clouds) through positive snow albedo feedback and land-atmosphere interactions (Bales et al., 2006; Dumont et al., 2020; Flanner et al., 2011; Gleason et al., 2019; Gul et al., 2021; Huang et al., 2022; Lee et al., 2017; Painter et al., 2010; Qian et al., 2015; Skiles et al., 2018; Yi et al., 2019). Snow albedo represents an important source of uncertainty in regional and global weather, climate, and hydrological modeling (Chen et al., 2014; Essery et al., 2009; He, Chen, et al., 2019; He et al., 2021; Oaida et al., 2015; Räisänen et al., 2017; Thackeray & Fletcher, 2016). Snow albedo is affected by many factors, including snow grain size and shape, snow depth, snow density, snow microstructure, snow surface roughness, light-absorbing particles (LAPs) present in the snowpack, the solar zenith angle, and the downward

solar spectrum (Dang et al., 2015; Dumont et al., 2021; Flanner et al., 2007, 2021; Gelman Constantin et al., 2020; He & Flanner, 2020; He, Takano, & Liou, 2017; He et al., 2014; Kokhanovsky & Zege, 2004; Liou et al., 2014; Picard et al., 2020; Wiscombe & Warren, 1980). Accurate simulation of snow albedo requires realistic characterization and physical representation of those key factors in land, weather, and climate models.

In the past decades, many empirical or semi-physical parameterizations have been developed to statistically link snow albedo with snowpack properties and environment conditions for application in weather and climate models (Abolafia-Rosenzweig et al., 2022; Gardner & Sharp, 2010; Roeckner et al., 2003; Verseghy, 1991; Vionnet et al., 2012; Yang et al., 1997), which however have their own limitations and uncertainties (He & Flanner, 2020). To achieve higher accuracy of snow albedo, several physics-based snowpack radiative transfer models have been developed, such as those based on the two-stream radiative transfer (Flanner et al., 2007; Libois et al., 2013; Tuzet et al., 2017), the Discrete-Ordinate-Method Radiative Transfer (DISORT) (Stamnes et al., 1988), the adding-doubling radiative transfer (Briegleb & Light, 2007; Dang et al., 2019), the Approximate Asymptotic Radiative Transfer (AART) Theory (Kokhanovsky & Zege, 2004; Libois et al., 2013), and the Monte Carlo Photon Tracing method (Kaempfer et al., 2007). Among them, the Snow, Ice, and Aerosol Radiative (SNICAR) model (Flanner et al., 2007, 2021) stands as one of the most widely used snowpack radiative transfer models, which has been implemented in several land and climate models including the Community Earth System Model (CESM)/Community Land Model (CLM; Lawrence et al., 2019) and the DOE's Energy Exascale Earth System Model (E3SM) Land Model (ELM; Golaz et al., 2019).

In previous snow radiative transfer models, it was a common practice to treat snow grains as spheres, externally mixed with LAPs such as black carbon (BC) and dust (Dang et al., 2015; Flanner et al., 2007; Tuzet et al., 2017; Warren & Wiscombe, 1980). However, in reality, snow grains are predominantly nonspherical, particularly for fresh snow (Dominé et al., 2003; Erbe et al., 2003). Additionally, BC and dust can be mixed within snow grains (i.e., internal mixing) rather than the common assumption that BC and dust only exist outside snow grains (i.e., external mixing) (Flanner et al., 2012; He, Liou, et al., 2019). To accurately compute snow albedo with more realistic representations of snow grain shape and its interaction with LAPs, physics-based parameterizations have been developed that account for snow nonsphericity and snow-LAP internal mixing for applications in weather and climate models (e.g., Dang et al., 2016; He, Takano, Liou, et al., 2017; He, Liou, et al., 2019; Räisänen et al., 2017; Saito et al., 2019), revealing important impacts of these two factors (He, 2022). In addition, the size, shape, and composition of LAPs play a nontrivial role in snow-LAP-radiation interactions (Flanner et al., 2021; He, Liou, & Takano, 2018, He, Liou, et al., 2019; Liou et al., 2014; Pu et al., 2021; Shi et al., 2022). Moreover, in addition to the traditionally modeled LAPs, such as BC and dust, there is increasing attention on other types of LAPs including brown carbon (Li et al., 2021; Liu et al., 2020; Yan et al., 2019), snow algae (Cook et al., 2017; Williamson et al., 2020), and volcanic ash (Flanner et al., 2014; Gelman Constantin et al., 2020; Young et al., 2014).

The standalone version of SNICAR has been updated to include several more realistic and physical treatments of snow-LAP-radiation interactions (updated version is SNICAR-ADv3; Flanner et al., 2021), including updated ice and aerosol optics as well as downward solar spectra, incorporation of multiple dust types and nonspherical snow grains, and the use of a more accurate adding-doubling (AD) two-stream radiative transfer solver. The standalone SNICAR-ADv3 model does not include BC/dust-snow internal mixing but uses a coated BC particle treatment instead, which shows similar effects as with explicit BC-snow internal mixing (Flanner et al., 2021). Leveraging the SNICAR-ADv3 updates and other aforementioned new LAP-snow parameterizations, the E3SM/ELM model with SNICAR as its embedded snow albedo scheme has been updated to include snow nonsphericity, BC/dust-snow internal mixing, and the adding-doubling radiative transfer solver, which leads to improved simulations of snow surface energy and water balances (Hao et al., 2023).

In view of the scientific and modeling advances, it is imperative to enhance the CESM/CLM-SNICAR snow albedo modeling with more realistic and physical representations of snow-LAP-radiation interactions, considering the broad use of CESM/CLM (Lawrence et al., 2019). The default CLM uses the original SNICAR model developed about 16 years ago (Flanner et al., 2007), which assumes spherical snow grains externally mixed with LAPs via a less accurate two-stream solver and outdated input databases for ice and aerosol optics and downward solar spectra. Similar to the standalone SNICAR model, the CLM-SNICAR uses a coated BC particle treatment to partially represent the effect of BC-snow internal mixing. These inadequate snow albedo treatments in CLM-SNICAR have been identified as a contributing factor to model biases in simulating surface albedo and snowpack evolution (e.g., Chen et al., 2014; Thackeray et al., 2019; Toure et al., 2018). Therefore, this study aims to

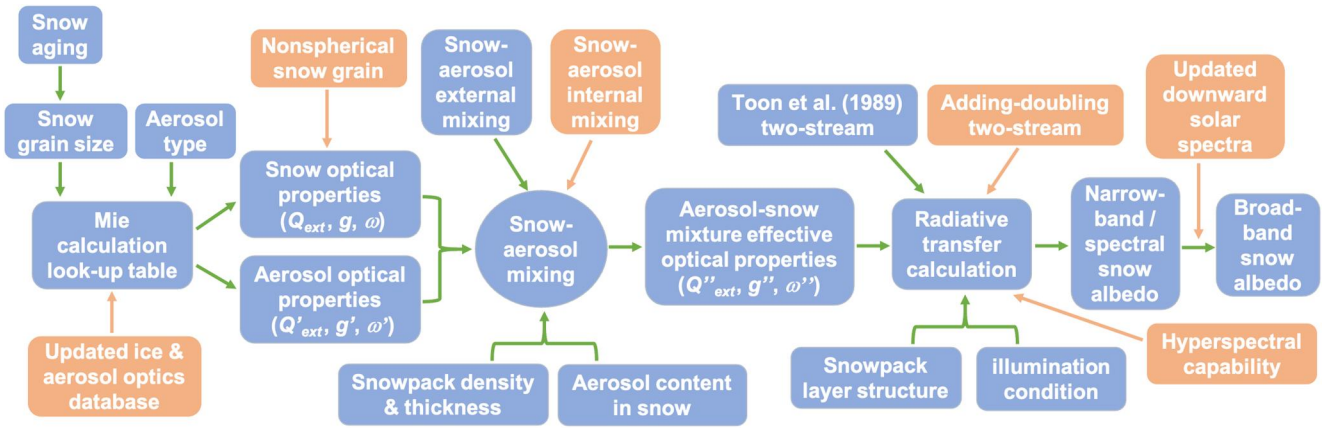

Figure 1. Workflow for key elements in CLM5-SNICAR snow albedo modeling. Blue boxes indicate the default model processes/capabilities. Orange boxes indicate the new model capabilities/enhancements implemented in this study. Q_{ext} is the mass extinction cross section, g is the asymmetry factor, and ω is the single-scattering albedo.

improve the CLM-SNICAR snow albedo scheme by incorporating more realistic and physically based representations of snow-LAP-radiation interactions.

This paper is organized as follows. Section 2 provides descriptions of model enhancements and simulations as well as observational data sets used for model evaluation. Section 3 investigates model sensitivities to each of the new features and enhancements implemented in this study. Section 4 presents evaluations of the updated model for key snow and surface fields. Section 5 concludes the study.

2. Model and Data

2.1. CLM5 Snow Albedo Scheme

We use the CLM version 5.0 (CLM5) in this study, which is the land component of CESM2. CLM5 represents a full suite of terrestrial biogeophysical and biogeochemical processes, including carbon and nitrogen cycles, vegetation dynamics for ecosystems, and land surface and subsurface energy and water processes. More details about CLM5 are provided in Lawrence et al. (2019). Since this study specifically focuses on snow albedo, we briefly summarize the key elements of the CLM5 snow albedo scheme below.

CLM5 includes the SNICAR model (Flanner et al., 2007) to compute snow albedo for the multi-layer (up to 12 layers) snowpack. It accounts for the effects of snow grain size (and hence snow aging) and LAP contamination on snow albedo. The original version of SNICAR leverages a multi-layer two-stream radiative transfer scheme based on Wiscombe and Warren (1980) and Toon et al. (1989). The required input variables for SNICAR include direct/diffuse radiation, surface downward solar spectrum, solar zenith angle (under direct radiation), ground albedo underlying snowpack, vertical distributions of snow grain size, snow layer thickness, snow density, aerosol concentration, and optical properties of ice and aerosols. The ice and aerosol optical properties (single-scattering albedo, mass extinction cross-section, and asymmetry factor) are computed offline by Mie theory using particle refractive indices and size distributions, and are archived as look-up tables. The BC and OC particle sizes are assumed to follow lognormal distributions with a number-median radius of 0.05 μm and geometric standard deviation of 1.5, and the dust particle radius is assumed to follow four size bins (0.05–0.5, 0.5–1.25, 1.25–2.5, and 2.5–5.0 μm). The CLM5-SNICAR assumes snow spheres externally mixed with aerosols. CLM-SNICAR assumes coated BC particles to partially mimic the effect of BC-snow internal mixing. In this study, to explicitly quantify the impact of BC-snow internal mixing, we did not include the coated BC treatment. The surface downward solar spectrum used in CLM5-SNICAR represents clear- or cloudy-sky atmospheric conditions typical of mid-latitude winter. The CLM5-SNICAR computes snow albedo at five spectral bands (300–700 nm, 700–1,000 nm, 1,000–1,200 nm, 1,200–1,500 nm, and 1,500–5,000 nm), which are then averaged to values at two broadbands (visible: 300–700 nm; near-infrared (NIR): 700–5,000 nm) weighted by the downward solar spectrum. More detailed descriptions of CLM-SNICAR can be found in Flanner et al. (2007). Figure 1 summarizes the general workflow for the key elements in CLM5-SNICAR snow albedo calculations.

Table 1
List of New Features and Enhancements in CLM-SNICAR Snow Albedo Scheme Implemented in This Study

Features/enhancements	New schemes & namelist options (* for new baseline)	Original scheme
Ice optical properties: updates from Flanner et al. (2021), with multiple options for ice refractive indices	snicar_snw_optics =	Warren (1984)
	1 (Warren, 1984; Perovich & Govoni, 1991)	
	2 (Warren & Brandt, 2008)	
	3* (Picard et al., 2016; Warren & Brandt, 2008)	
BC and OC optical properties: updates from Flanner et al. (2021)	Flanner et al. (2021)	Flanner et al. (2007)
Dust optical properties: updates from Flanner et al. (2021) with multiple dust types	snicar_dust_optics =	Saharan dust (Flanner et al., 2007)
	1* (Saharan dust)	
	2 (Colorado dust)	
	3 (Greenland dust)	
Downward solar spectra: updates from Flanner et al. (2021) for multiple atmospheric conditions	snicar_solarspec =	Mid-latitude winter (Flanner et al., 2007)
	1* (Mid-latitude winter)	
	2 (Mid-latitude summer)	
	3 (Sub-Arctic winter)	
	4 (Sub-Arctic summer)	
	5 (Summit, Greenland)	
	6 (High mountain)	
Radiative transfer solver: new adding-doubling solver from Dang et al. (2019)	snicar_rt_solver =	Toon et al. (1989)
	1 (Toon et al., 1989)	
	2* (Adding-Doubling)	
Snow grain shape: nonspherical snow grains from He, Takano, Liou, et al. (2017)	snicar_snw_shape =	Sphere
	1 (Sphere)	
	2 (Spheroid)	
	3* (Hexagonal)	
	4 (Snowflake)	
BC-snow mixing: internal mixing from He, Takano, Liou, et al. (2017)	snicar_snobc_intmix =	External mixing
	True (internal mixing)	
	False* (external mixing)	
Dust-snow mixing: internal mixing from He, Liou, et al. (2019)	snicar_snodst_intmix =	External mixing
	True (internal mixing)	
	False* (external mixing)	
Wavelength band: new hyperspectral (480-band, 10-nm spectral resolution) capability from Flanner et al. (2021)	snicar_numrad_snw =	5-band
	5* (5-band)	
	480 (480-band)	
New namelist controls for aerosol & OC	snicar_use_aerosol = true*, false	No namelist controls on using aerosol and OC (hard-coded)
	DO_SNO_OC = true, false*	

2.2. New Features and Enhancements in CLM5 Snow Albedo Scheme

The standalone version of SNICAR has been recently updated to SNICAR-ADv3 by Flanner et al. (2021) with several new features as mentioned in Section 1. In addition, new parameterizations that account for BC-snow and dust-snow internal mixing have been recently developed. Thus, we combine all these recent updates that more physically and realistically represent snowpack characteristics in snow albedo computation, and implement them into CLM5-SNICAR (Table 1 and Figure 1). Particularly, we include these new features/enhancements as additional CLM5-SNICAR physics/namelist options, which offers an effective way to quantify model sensitivity

to snow albedo processes and allows for relevant multi-physics model ensemble analyses for uncertainty evaluation. We note that the new default setting selected for each physics/namelist option in the following subsections mainly follows SNICAR-ADv3 (Flanner et al., 2021), which represents more accurate particle properties and radiative transfer calculations and/or is more representative of typical application conditions. However, we realize that these default option selections are still arbitrary to some extent, and users have the freedom to use different options for specific applications.

2.2.1. Updated Ice Optical Properties

The original CLM5-SNICAR uses the Warren (1984) compilation of ice refractive indices (RI) across the solar spectrum. Later, Warren and Brandt (2008) further updated the ice refractive indices data with much weaker absorption at wavelengths below 600 nm. However, more recent measurements by Picard et al. (2016) showed a larger ice absorption (i.e., the imaginary part of refractive indices) at 320–600 nm wavelengths than the Warren and Brandt (2008) data but smaller than the Warren (1984) data. This is consistent with the systematic snow albedo overestimate at wavelengths below 500 nm in SNICAR simulations using the Warren and Brandt (2008) data (He, Flanner, et al., 2018). Thus, Flanner et al. (2021) updated the imaginary part of ice refractive indices by replacing the Warren and Brandt (2008) data with the Picard et al. (2016) data at wavelengths shorter than 600 nm. Flanner et al. (2021) also compiled another data set for the imaginary part of ice refractive indices by merging the Warren (1984) and Perovich and Govoni (1991) data sets. These three data sets use the same Warren and Brandt (2008) compilation of the real part of refractive indices, and only differ in the imaginary part at wavelengths less than 600 nm, which is extremely challenging to measure accurately. Including all these three data sets in CLM5-SNICAR (i.e., ice optics namelist option "snicar_snw_optics" in Table 1) will allow uncertainty quantification. Following Flanner et al. (2021), we use the merged Picard et al. (2016) data set as the new baseline model option in the updated CLM5-SNICAR.

Using the ice refractive indices, ice optical properties (i.e., single-scattering albedo, mass extinction cross-section, and asymmetry factor) are then computed by Mie theory based on various spherical ice grain effective radii ranging from 30 to 1,500 μm with lognormal size distributions (Flanner et al., 2021), and are archived as an input look-up table. We note that Mie theory cannot treat nonspherical snow grain shape, which is accounted for via a parameterization that makes corrections to the asymmetry factor of snow spheres in the updated CLM5-SNICAR (see Section 2.2.6 for details). The look-up table of ice optical properties created by Flanner et al. (2021) is for 480-band at 10-nm spectral (i.e., hyperspectral) resolution across the solar spectrum (200–5,000 nm). To work with the five spectral bands in CLM5-SNICAR, we further use the spectral weighted averaging technique to convert the hyperspectral ice optical properties to the 5-band values following Flanner et al. (2007). For the new hyperspectral computation option added to CLM5-SNICAR (see Section 2.2.9), we directly use the 480-band ice optics data set produced by Flanner et al. (2021).

2.2.2. Updated Aerosol Optical Properties

The original CLM5-SNICAR accounts for three types of LAPs, including BC, OC (i.e., brown carbon), and dust (Saharan type), using the aerosol optics data set developed by Flanner et al. (2007). Flanner et al. (2021) updated the optical properties for all three aerosol types using updated particle density, size distribution, and refractive indices via Mie theory calculations. Overall, the updated aerosol optical properties lead to a stronger light absorption for OC and Saharan dust but a weaker light absorption for BC. We implement the Flanner et al. (2021) data set into CLM5-SNICAR and conduct the spectral weighted averaging to convert the hyperspectral (480-band) aerosol optical properties to the 5-band values following Flanner et al. (2007). For the new hyperspectral computation option (see Section 2.2.9), we directly use the 480-band aerosol optics data set (Flanner et al., 2021). Given the substantial uncertainty in OC modeling due to a lack of observational constraints (Liu et al., 2020), we turn off the OC effect on snow albedo (namelist option "DO_SNO_OC" in Table 1) in our proposed new baseline model configuration, but we activate it in sensitivity simulations to test its impact (Section 3).

2.2.3. Updated Dust Types

The original CLM5-SNICAR only accounts for one dust type (i.e., Saharan dust; Flanner et al., 2007), while previous studies showed substantial differences in dust optical properties due to different particle size and composition for dust that originates from different regions (Polashenski et al., 2015; Scanza et al., 2015; Skiles &

Painter, 2017). Thus, in addition to the Saharan dust (Scanza et al., 2015), Flanner et al. (2021) included two more dust types, Colorado dust (Skiles & Painter, 2017) and Greenland dust (Polashenski et al., 2015), which are added to the updated CLM5-SNICAR in this study. Overall, Greenland dust shows the strongest light absorbing ability, followed by Saharan dust, while Colorado dust has the weakest light absorbing capacity among the three (Flanner et al., 2021). Including different dust types in CLM5-SNICAR (i.e., dust optics namelist option "snicar_dust_optics" in Table 1) offers a way for uncertainty analysis. Following Flanner et al. (2021), we use the Saharan dust as the new baseline model option in the updated CLM5-SNICAR. We note that the updated model does not have the capability of simultaneously using multiple dust types over different regions in one single simulation. Ideally, the CLM5-SNICAR should be able to take the spatiotemporally varying aerosol optical properties (dust, BC, and OC) directly from the coupled atmospheric model component for consistent simulations, which will be improved in the future.

2.2.4. Updated Surface Downward Solar Spectra

The original CLM5-SNICAR uses the surface downward solar spectrum for clear-sky or cloudy-sky atmospheric conditions typical of mid-latitude winter (Flanner et al., 2007). In the model, the downward solar spectrum is used uniformly across the simulation domain to compute the spectrally integrated broadband snow albedo from the spectral albedo derived from the radiative transfer solver. However, atmospheric conditions significantly affect the downward solar spectrum at the surface and therefore using only one downward solar spectrum may lead to nontrivial errors in simulated broadband snow albedo. Thus, Flanner et al. (2021) developed five additional downward solar spectra to represent clear-sky and cloudy-sky atmospheric conditions typical of mid-latitude summer, sub-Arctic winter, sub-Arctic summer, Summit Greenland, and high mountain environments. We implement these new downward solar spectra (i.e., solar spectrum namelist option "snicar_solarspec" in Table 1) into CLM5-SNICAR to offer more accurate albedo calculations for applications in those specific regions. Following Flanner et al. (2021), we use the mid-latitude winter spectrum as the new baseline model option in the updated CLM5-SNICAR. We note that the updated model does not have the capability of simultaneously using multiple solar spectra over different regions in one single simulation. Ideally, the CLM5-SNICAR should be able to take the spatiotemporally varying downward solar spectrum directly from the coupled atmospheric model component for consistent simulations. This is an important opportunity for further future improvement.

2.2.5. Updated Radiative Transfer Solver

The original CLM5-SNICAR adopts the tri-diagonal matrix two-stream solver (Toon et al., 1989), which shows larger snow albedo biases (i.e., overestimates) particularly under diffuse conditions than an adding-doubling two-stream solution (Dang et al., 2019). Moreover, the adding-doubling solution has a stronger computational stability under different solar zenith angles and a higher computational efficiency than the tri-diagonal matrix solution. The adding-doubling solver also allows accounting for internal Fresnel layers in snow-ice interface, providing the potential for a unified snow-ice radiative transfer treatment. Because of these advantages, the adding-doubling solution has been implemented in the standalone SNICAR-ADv3 (Flanner et al., 2021) and the E3SM/ELM model (Hao et al., 2023). Following these recent studies, we implement the adding-doubling solution into CLM5-SNICAR (i.e., radiative transfer namelist option "snicar_rt_solver" in Table 1), and use it as the new baseline model option in the updated CLM5-SNICAR, considering its higher computational accuracy, efficiency, and stability (supercomputer used in this study: SGI 5.34-petaflops high-performance computer with Intel Xeon processor cores; https://arc.ucar.edu/knowledge_base/70549542). Detailed descriptions of the adding-doubling formulation can be found in Dang et al. (2019).

2.2.6. Representation of Snow Nonsphericity

The original CLM5-SNICAR assumes spherical snow grains (Flanner et al., 2007), which however may not be a realistic representation since nonspherical snow grains are ubiquitous in reality (Dominé et al., 2003; Erbe et al., 2003). To quantify the impact of snow nonsphericity, He, Takano, Liou, et al. (2017) developed a set of snow optical parameterizations based on sophisticated geometric-optics ray-tracing calculations (Liou et al., 2014) for four typical snow grain shapes representative of real-world observations, including sphere, spheroid, hexagonal plate/column, and fractal snowflake (Figure 2). Snow grain shape mainly affects the snow asymmetry factor with very limited impact on extinction cross section and single-scattering albedo (Dang et al., 2016; He & Flanner, 2020). Thus, the He, Takano, Liou, et al. (2017) parameterizations make corrections to

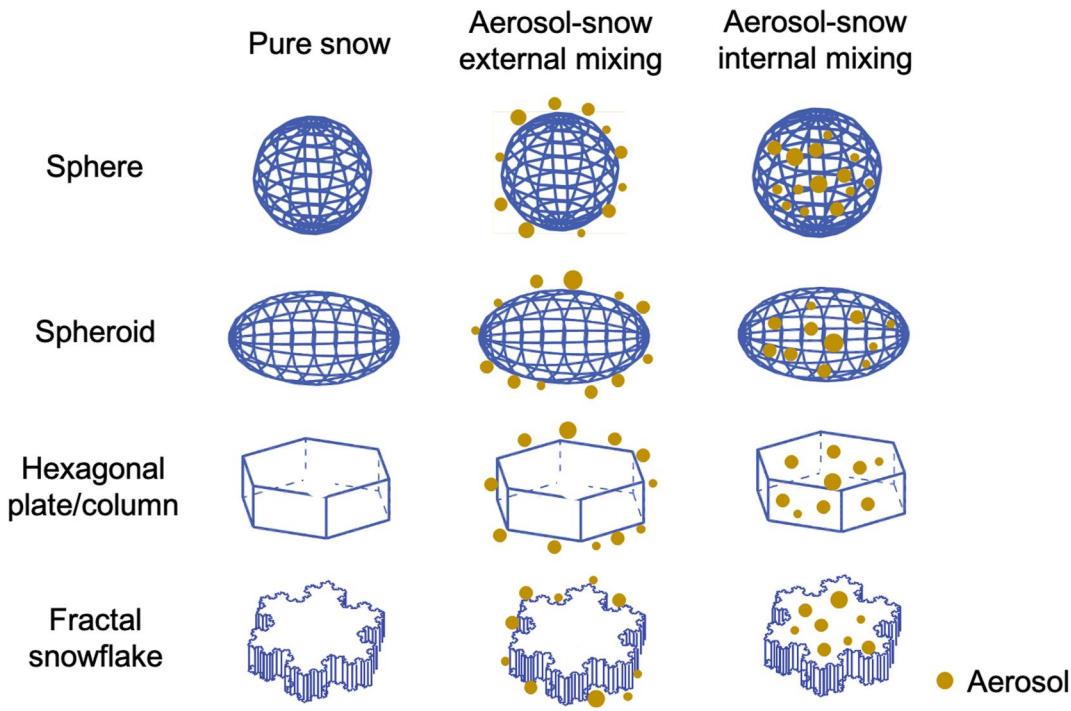

Figure 2. Demonstration of snow grains with four different shapes as well as aerosol-snow external and internal mixing states that are implemented in this study.

the asymmetry factor of snow spheres to account for nonsphericity effects based on grain shape, aspect ratio, effective radius, and wavelength. The parameterizations have been implemented into the standalone SNICAR-ADv3 (Flanner et al., 2021) and the E3SM/ELM model (Hao et al., 2023), which provide detailed descriptions of the associated formulation and implementation. Following these recent studies, we implement the same parameterizations for the four grain shapes into CLM5-SNICAR (i.e., snow shape namelist option "snicar_snw_shape" in Table 1). We set the hexagonal shape (one of the most common shapes for ice crystal; Liou et al., 2014; Flanner et al., 2021) as the new baseline model option in the updated CLM5-SNICAR.

We note that there are other parameterizations that account for nonspherical snow grains in albedo calculations, which have been used in other land/climate models (e.g., Libois et al., 2013; Räisänen et al., 2017; Saito et al., 2019). These studies all find that accounting for snow nonsphericity provides a more realistic representation of snow characteristics in albedo calculations. All of these models are limited by a lack of dynamic evolution of snow grain shapes, which is another opportunity for future model development. We note that in this study, the snow aging scheme that simulates the dynamic evolution of specific surface area (Flanner et al., 2007) is the same as that in the default CLM-SNICAR. Thus, the snow nonsphericity effect analyzed here quantifies the impact of different grain shapes with equal specific surface area. A recent study (Robledano et al., 2023) found that the optical properties of natural snow can be represented using a collection of non-symmetrical convex particle, where two main optical shape parameters (absorption enhancement parameter and geometric asymmetry parameter) are used to characterize the optical shape effect. Their measurements of natural snow provided an accurate estimate of the range of these optical parameters, which can be applied to climate models for a more realistic snow representation.

2.2.7. Representation of BC-Snow Internal Mixing

The original CLM5-SNICAR assumes BC-snow external mixing, with hydrophilic BC treated as coated BC. However, previous studies pointed out that BC can also be internally mixed with snow grains (Figure 2), through a number of BC-cloud-precipitation interaction processes, which strongly enhances BC-induced snow albedo reduction (Flanner et al., 2012; He, Takano, Liou, et al., 2017; Liou et al., 2014). He, Takano, Liou, et al. (2017) developed a parameterization to account for BC-snow internal mixing in snow albedo calculations, where the

internal mixing mainly affects the single-scattering albedo of BC-snow mixtures with negligible impacts on snow asymmetry factor and extinction cross section. This parameterization was developed based on sophisticated geometric-optics ray-tracing calculations and computes the change of snow single-scattering albedo caused by BC-snow internal mixing as a function of BC particle effective radius and concentration in snow. This parameterization was implemented into an earlier version of SNICARv2 (He, Flanner, et al., 2018), which describes the formulation and implementation in detail. Following He, Flanner, et al. (2018), we implement the BC-snow internal mixing parameterization into CLM5-SNICAR (i.e., BC-snow mixing namelist option "snicar_snobc_intmix" in Table 1), assuming hydrophilic BC to be internally mixed with snow. We note that there is a lack of observational constraints for BC-snow mixing state (internal vs. external) and there is also substantial uncertainty in modeling the evolution of BC-snow mixing state, therefore we maintain the BC-snow external mixing as the new baseline model option in the updated CLM5-SNICAR, but we activate the internal mixing in sensitivity simulations to quantify its impact (Section 3). We also note that in this study, we do not include the coated BC treatment, because the soluble aerosol constituents coated on BC particle surfaces are likely dissolved into hydrometeors during BC wet deposition (He, 2022).

There are other methods developed to account for the effect of BC-snow internal mixing, such as the look-up table method developed based on a dynamic effective medium approximation in Flanner et al. (2012), which has been adopted by E3SM/ELM-SNICAR (Hao et al., 2023). He, Flanner, et al. (2018) showed that the He, Takano, Liou, et al. (2017) parameterization of BC-snow internal mixing leads to consistent snow albedo reductions with the results computed from the Flanner et al. (2012) look-up tables. More observations of BC-snow mixing state are needed to constrain models to achieve more accurate estimates of BC-induced snow albedo changes.

2.2.8. Representation of Dust-Snow Internal Mixing

Similar to the BC-snow mixing treatment, the original CLM5-SNICAR assumes dust-snow external mixing. However, previous studies found that dust can also be mixed internally with snow grains (Figure 2) via dust-cloud-precipitation interactions, which enhances dust-induced snow albedo reduction (He, Liou, et al., 2019; Shi et al., 2021). To quantify the impact of dust-snow internal mixing, He, Liou, et al. (2019) developed a parameterization that nonlinearly connects internal mixing-induced changes of snow single-scattering albedo to dust concentration in snow based on sophisticated geometric-optics ray-tracing calculations. The dust-snow internal mixing has negligible effects on the snow asymmetry factor and extinction cross section. The He, Liou, et al. (2019) parameterization was implemented into E3SM/ELM-SNICAR (Hao et al., 2023). In the present study, we implement the dust-snow internal mixing parameterization into CLM5-SNICAR (i.e., dust-snow mixing namelist option "snicar_snodst_intmix" in Table 1). Similar to BC-snow mixing, there is also a lack of observational constraints for dust-snow mixing state and large model uncertainty for the mixing state evolution. Thus, we maintain the dust-snow external mixing as the new baseline model option in the updated CLM5-SNICAR, but we activate the internal mixing in sensitivity simulations to test its impact (Section 3). We note that the He, Liou, et al. (2019) parameterization of dust-snow internal mixing was developed without the presence of internally mixed BC, so we suggest not activating BC-snow and dust-snow internal mixing simultaneously in CLM5-SNICAR.

Recently, Shi et al. (2021) used another method (i.e., the effective medium approximation) to account for dust-snow internal mixing in snow albedo modeling, which shows generally consistent results with those derived from the He, Liou, et al. (2019) parameterization. In the future, more observations of dust-snow mixing state are needed to better constrain modeled dust impacts on snow albedo.

2.2.9. New Hyperspectral Computation Capability

The original CLM5-SNICAR uses five spectral bands (300–700 nm, 700–1,000 nm, 1,000–1,200 nm, 1,200–1,500 nm, and 1,500–5,000 nm) in radiative transfer calculations to increase computational efficiency. Accordingly, the ice and aerosol optical properties and downward solar spectra in input data sets are all spectrally averaged into the five bands. However, a recent study (Wang et al., 2022) found that because of the nonlinearity of radiative transfer computation, using the five spectral bands in SNICAR leads to a nontrivial snow albedo bias (up to 0.05) compared to hyperspectral (10-nm spectral resolution) calculations. Wang et al. (2022) further developed a set of corrected 5-band mean ice and aerosol single-scattering properties that reduce the albedo bias, which however were based on the old SNICAR optical data sets and hence are not used in this study for the 5-band

calculations. Instead, we implement a hyperspectral (10-nm spectral resolution with 480 bands) computation capability into CLM5-SNICAR in this study, similar to that used by the standalone SNICAR-ADv3 model. The hyperspectral modeling capability includes all the new features and enhancements mentioned in Sections 2.2.1–2.2.8. The addition of this hyperspectral capability particularly targets on local/regional process-level investigations that require higher snow albedo accuracy, because it is much more computationally expensive than the 5-band calculations (e.g., 8 times slower for global 1-deg 10-year simulations in this study using the configuration described in Section 2.3).

2.3. Model Simulations

To assess the model sensitivities and performance with the aforementioned new features and enhancements, we conduct a series of global 1-deg land-only CLM5-SNICAR simulations driven by the atmospheric forcing from the 3-hourly 0.5° Global Soil Wetness Project Phase 3 data set (GSWP3; Dirmeyer et al., 2006), which has been widely used and evaluated by previous studies (e.g., Hao et al., 2023; Lawrence et al., 2019). All model simulations use the prescribed monthly climatological MODIS satellite phenology mode (i.e., CLM configuration/compset: I2000Clm51Sp) (Lawrence et al., 2019), and the prescribed monthly aerosol (BC, dust, OC) wet and dry deposition flux from the CESM2-WACCM simulations participated in CMIP6 experiments (Danabasoglu et al., 2020).

Model experiments include a default baseline simulation using the original CLM5-SNICAR (hereinafter "default baseline"), a new baseline simulation using the enhanced CLM5-SNICAR (hereinafter "new baseline") with the new baseline physics option identified above and in Table 1, and a set of twin sensitivity simulations by turning on and off each new feature/enhancement (Table 1) at a time with the same baseline setup for other snow physics options in order to quantify the impact of the targeted feature/enhancement. The aerosol-induced snow albedo radiative forcing analyzed in this study is based on the instantaneous ground net radiative flux difference through double calls of SNICAR with and without specific aerosol species. We spin up the model simulations for the years 2000–2005 and use the 2006–2010 period for analysis. For seasonal analysis, we define each season as winter (December–January–February), spring (March–April–May), summer (June–July–August), and fall (September–October–November).

2.4. Data for Model Evaluation

To evaluate the default and new baseline model simulations of snow albedo and other snowpack properties, global spatiotemporally continuous observation-based data sets are preferred. Thus, we use the daily 0.05° MODIS data for snow cover fraction (MOD10C1 and MYD10C1) and surface albedo (MCD43C3) as well as the monthly 0.1° ERA–5 land reanalysis data (hereinafter ERA5-Land) for snow water equivalent (SWE), snow depth, and surface (2-m) air temperature. The MODIS MCD43C3 product is an Aqua-Terra merged surface albedo data set and we use the data with quality flag of 0–2 (i.e., "ok," "good," and "best") to achieve a balance between enough samples and data quality, following He, Chen, et al. (2019). We use the MODIS snow cover data with quality flag of 0 and 1 (i.e., "good" and "best") and cloud fraction of <20% (more clouds lead to degraded data accuracy) to achieve a balance between enough samples and data quality, following He, Chen, et al. (2019). We further merge the Aqua (MYD10C1) and Terra (MOD10C1) MODIS snow cover data to obtain more complete global maps by replacing the data gaps in MOD10C1 with valid values (if existing) from MYD10C1 or averaging the pixel values if both MOD10C1 and MYD10C1 have valid data. To compare with model simulations at consistent spatial grids, we remap the MODIS and ERA5-Land data to the model grids by averaging the values across the MODIS 0.05° pixels and ERA5-Land 0.1° pixels that are within each of the model 1° grids, respectively.

3. Model Sensitivities to New Features/Enhancements

3.1. Effects of Updated Ice Optics

Figure 3 shows the all-sky annual mean effects of updated ice optical properties on global snow albedo by using the Picard et al. (2016) versus Warren and Brandt (2008) visible ice refractive indices. The differences in visible snow albedo are small (<0.005) with slightly lower albedo using the Picard et al. (2016) data mainly over two polar regions (Figure 3 and Figure S1 in Supporting Information S1; Table 2). This is because the Picard et al. (2016) data leads to a stronger visible ice absorption (Flanner et al., 2021). Because the two refractive index data sets only differ in the UV/visible band, the minor difference in the NIR albedo (mainly in the mid-latitudes) is

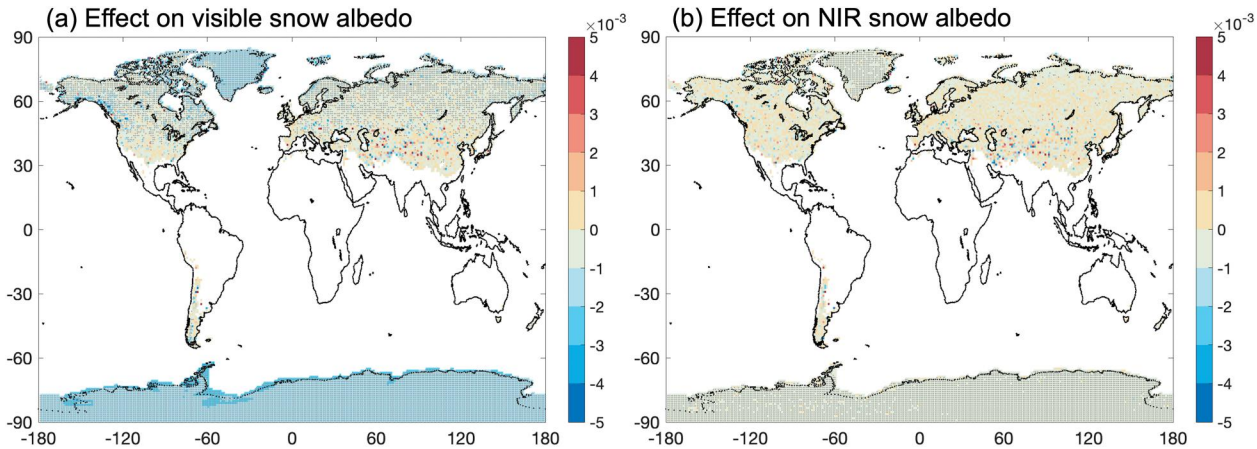

Figure 3. 5-year (2006–2010) all-sky annual mean effects of updated ice optical properties (i.e., differences between simulations using the Picard et al. (2016) and Warren and Brandt (2008) ice refractive indices): (a) difference for visible snow albedo, (b) difference for NIR snow albedo. Regions with statistically significant differences ($p < 0.05$) are marked by gray "+" symbols.

due to slight changes in other snow properties such as grain size, snow density, and/or snowpack thickness, which also contribute to the visible snow albedo differences (statistically insignificant) in the mid-latitudes (Figure 3 and Figure S1 in Supporting Information S1). Due to the relatively small differences in both visible and NIR bands, the annual mean difference in the shortwave snow albedo is also negligible across different latitudes (Table 2). Although the impact of using the Picard et al. (2016) data is small, it appears to more accurately capture the ice absorption in the visible band (Flanner et al., 2021; He, Flanner, et al., 2018) and hence is recommended for use in future studies.

3.2. Effects of Updated Aerosol Optics

Figure 4 shows the all-sky annual mean effects of updated aerosol (BC, OC, and Saharan dust) optical properties from the Flanner et al. (2021) data versus the Flanner et al. (2007) data on snow-covered (0%< snow cover ≤100%) ground albedo and corresponding aerosol-induced grid-mean snow albedo radiative forcing. Compared to using the Flanner et al. (2007) aerosol optics, the total aerosol-induced snow-covered ground albedo reduction using the Flanner et al. (2021) data is enhanced by up to 0.02 mainly over northern mid-latitudes and

Table 2
Effects of Model Sensitivity Factors on Global Land Snow Albedo

		All-sky annual shortwave snow albedo				
Sensitivity factors		Northern high-latitudes (90°N–60°N)	Northern mid-latitudes (60°N–30°N)	Low-latitudes (30°N–30°S)	Southern mid-latitudes (30°S–60°S)	Southern high-latitudes (60°S–90°S)
Ice refractive index (Section 3.1)	Picard et al. (2016)	0.699	0.522	0.220	0.247	0.851
	Warren and Brandt (2008)	0.699	0.522	0.220	0.247	0.851
Downward solar spectrum (Section 3.4)	High mountain	0.691	0.517	0.219	0.245	0.842
	Mid-latitude summer	0.704	0.526	0.222	0.248	0.855
Radiative transfer solver (Section 3.5)	Adding-doubling	0.699	0.522	0.220	0.247	0.851
	Toon et al. (1989)	0.688	0.518	0.219	0.244	0.842
Snow grain shape (Section 3.6)	Snowflake	0.748	0.573	0.252	0.280	0.884
	Sphere	0.699	0.522	0.220	0.247	0.851
Spectral resolution (Section 3.9)	480-band	0.697	0.521	0.219	0.245	0.851
	5-band	0.698	0.522	0.220	0.247	0.851

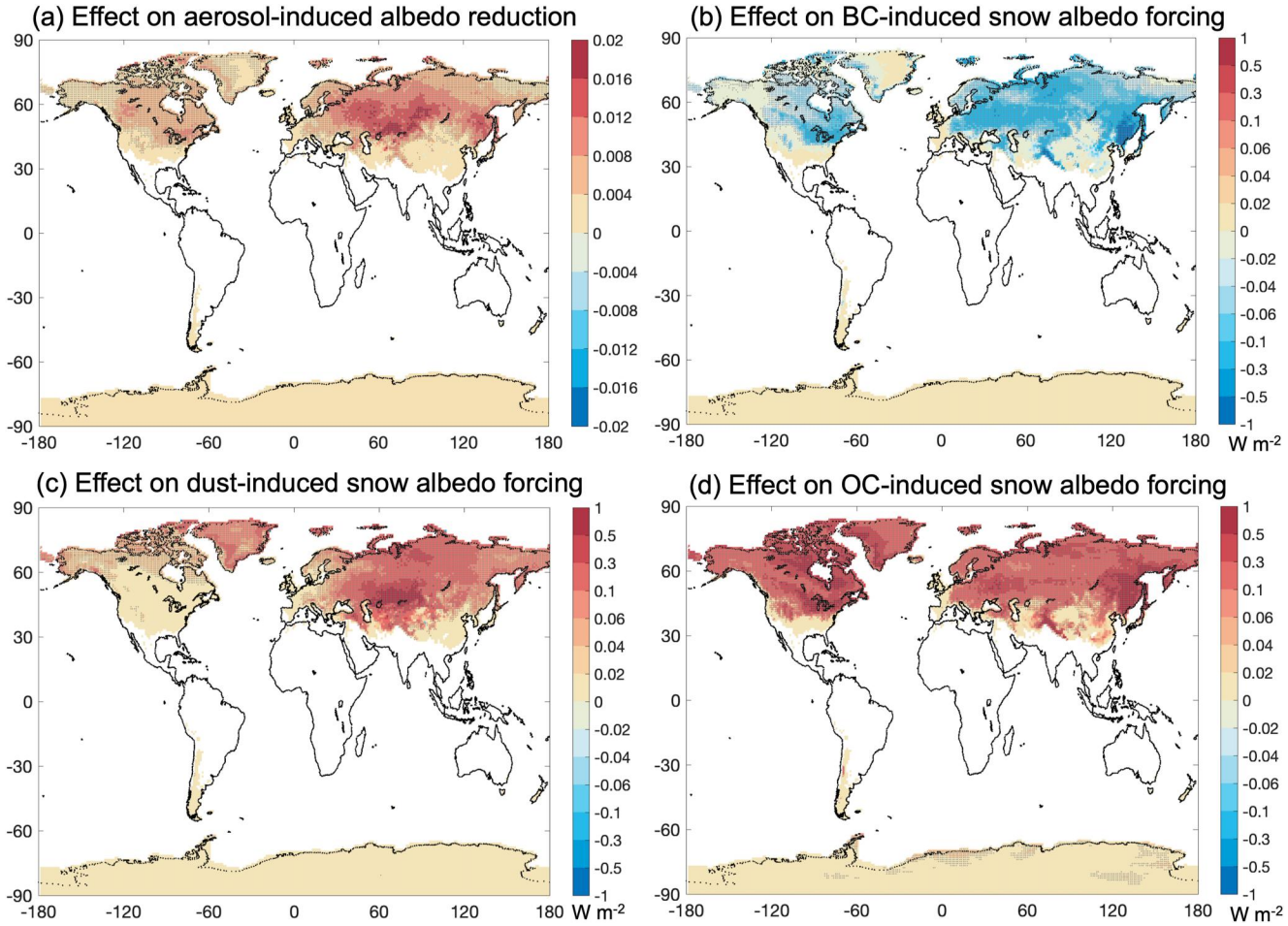

Figure 4. 5-year (2006–2010) all-sky annual mean effects of updated aerosol optical properties (i.e., differences between simulations using the Flanner et al. (2007, 2021) data): (a) difference for snow-covered (0%< snow cover ≤100%) ground albedo reduction caused by all aerosols, (b) difference for BC-induced grid-mean snow albedo forcing (W m^{-2}), (c) difference for dust-induced grid-mean snow albedo forcing (W m^{-2}), (d) difference for OC-induced grid-mean snow albedo forcing (W m^{-2}). Regions with statistically significant differences ($p < 0.05$) are marked by gray "+" symbols.

high-latitudes (Figure 4a). This is primarily driven by stronger dust and OC light absorption in the Flanner et al. (2021) data relative to the Flanner et al. (2007) data, which further leads to stronger induced grid-mean snow albedo forcing (dust and OC combined) by up to >2.0 W m^{-2} over heavily polluted hotspots, and by about 0.31 and 0.15 W m^{-2} averaged over the Northern Hemispheric and global snowpack, respectively (Figures 4c and 4d and Table 3). We note that the largely enhanced OC albedo forcing is due to the use of relatively strong-absorbing brown carbon optics in Flanner et al. (2021), which may not be representative of all OC or brown carbon. The enhanced snow albedo forcing caused by dust and OC is partially offset by the weaker BC light absorption with the BC-induced snow albedo forcing reduced by about 0.06 and 0.03 W m^{-2} averaged over the Northern Hemispheric and global snowpack, respectively (Figure 4b and Table 3). The differences caused by updated aerosol optics mainly occur over northern mid-latitudes during winter and spring, and northern high-latitudes during spring and summer (Figure S2 in Supporting Information S1).

3.3. Effects of Different Dust Types

Figure 5 shows the all-sky annual mean differences between simulations using Greenland dust and Colorado dust in snow-covered (0%< snow cover ≤100%) ground albedo reduction and grid-mean snow albedo forcing caused by dust. These two types of dust show the largest difference in light absorption capabilities among all the three dust types in the model (Section 2.2.3), which demonstrates the upper limit of model sensitivity to dust types in CLM5. Overall, using Greenland dust shows stronger albedo reduction by up to 0.02 mainly over northern

Table 3
Effects of Model Sensitivity Factors on Global Land Aerosol-Induced Snow Albedo Forcing

Sensitivity factors		Aerosol-induced annual snow albedo forcing (W m^{-2})[a]				
		Northern high-latitudes (90°N–60°N)	Northern mid-latitudes (60°N–30°N)	Low-latitudes (30°N–30°S)	Southern mid-latitudes (30°S–60°S)	Southern high-latitudes (60°S–90°S)
BC						
Aerosol optics (Section 3.2)	Flanner et al. (2021)	0.21	0.23	0.04	~0.00	0.01
	Flanner et al. (2007)	0.26	0.31	0.06	~0.00	0.01
Dust type (Section 3.3)	Greenland dust	0.20	0.22	0.04	~0.00	0.01
	Colorado dust	0.22	0.24	0.04	~0.00	0.01
Snow grain shape (Section 3.6)	Snowflake	0.16	0.19	0.04	~0.00	0.01
	Sphere	0.20	0.23	0.04	~0.00	0.01
BC-snow mixing (Section 3.7)	Internal mixing	1.20	1.09	0.14	0.01	0.31
	External mixing	0.21	0.23	0.04	~0.00	0.01
Dust-snow mixing (Section 3.8)	Internal mixing	0.17	0.20	0.03	~0.00	0.01
	External mixing	0.20	0.23	0.04	~0.00	0.01
Spectral resolution (Section 3.9)	480-band	0.21	0.23	0.04	~0.00	0.02
	5-band	0.20	0.23	0.04	~0.00	0.01
Dust						
Aerosol optics (Section 3.2)	Flanner et al. (2021)	0.26	0.28	0.01	~0.00	0.01
	Flanner et al. (2007)	0.16	0.19	0.01	~0.00	~0.00
Dust type (Section 3.3)	Greenland dust	0.34	0.28	0.02	~0.00	0.01
	Colorado dust	0.12	0.19	0.01	~0.00	~0.00
Snow grain shape (Section 3.6)	Snowflake	0.20	0.25	0.01	~0.00	~0.00
	Sphere	0.26	0.27	0.02	~0.00	0.01
BC-snow mixing (Section 3.7)	Internal mixing	0.15	0.15	~0.00	~0.00	0.01
	External mixing	0.26	0.27	0.01	~0.00	0.01
Dust-snow mixing (Section 3.8)	Internal mixing	0.63	0.51	0.03	~0.00	0.12
	External mixing	0.26	0.27	0.01	~0.00	0.01
Spectral resolution (Section 3.9)	480-band	0.25	0.25	0.01	~0.00	0.01
	5-band	0.26	0.27	0.01	~0.00	0.01
OC						
Aerosol optics (Section 3.2)	Flanner et al. (2021)	0.32	0.28	0.04	~0.00	0.01
	Flanner et al. (2007)	0.04	0.04	0.01	~0.00	~0.00
Dust type (Section 3.3)	Greenland dust	0.30	0.26	0.03	~0.00	0.01
	Colorado dust	0.33	0.30	0.04	~0.00	0.01
Snow grain shape (Section 3.6)	Snowflake	0.25	0.23	0.04	~0.00	0.01
	Sphere	0.31	0.27	0.04	~0.00	0.01
BC-snow mixing (Section 3.7)	Internal mixing	0.19	0.13	0.01	~0.00	0.01
	External mixing	0.31	0.27	0.04	~0.00	0.01
Dust-snow mixing (Section 3.8)	Internal mixing	0.26	0.23	0.03	~0.00	0.01
	External mixing	0.31	0.27	0.04	~0.00	0.01

Table 3
Continued

Sensitivity factors		Aerosol-induced annual snow albedo forcing (W m^{-2})[a]				
		Northern high-latitudes (90°N–60°N)	Northern mid-latitudes (60°N–30°N)	Low-latitudes (30°N–30°S)	Southern mid-latitudes (30°S–60°S)	Southern high-latitudes (60°S–90°S)
Spectral resolution (Section 3.9)	480-band	0.37	0.31	0.04	~0.00	0.02
	5-band	0.31	0.27	0.04	~0.00	0.01

[a]Aerosol-induced snow albedo forcing is averaged over snow-covered (0%< snow cover ≤100%) land grids for each latitudinal band. Values within −0.005 ~ 0.005 are marked as "~0.00."

Eurasia during winter and spring (Figure 5a and Figure S3 in Supporting Information S1), compared to using Colorado dust. The corresponding annual difference in dust-induced grid-mean snow albedo forcing reaches more than 1.0 W m^{-2} over polluted hotspots, with about 0.2 and 0.1 W m^{-2} averaged over the Northern Hemispheric and global snowpack, respectively (Figure 5b and Table 3). Seasonally, the differences in snow albedo forcing mainly locate in northern mid-latitudes during winter and spring, and northern high-latitudes during spring and summer (Figure S4 in Supporting Information S1). The enhanced light absorption by Greenland dust relative to Colorado dust also leads to reduced light absorption and hence lower snow albedo forcing caused by BC and OC (by 0.012–0.015 W m^{-2} over the global snowpack) (Table 3).

3.4. Effects of Updated Downward Solar Spectra

Figure 6 shows the 5-year annual mean effects of downward solar spectra on snow albedo by using the high mountain spectrum versus the mid-latitude summer spectrum. These two spectra have the largest difference in energy distribution in the CLM5 spectral bands particularly for direct radiation (Figure S5 in Supporting Information S1), which demonstrates the upper limit of model sensitivity to downward solar spectra. Specifically, the snow albedo difference (by up to −0.03) between using the two spectra primarily occurs in the NIR band under direct radiation (Figure 6c), particularly over high latitudes with a mean difference of about −0.01 (Table 2). This is because the high mountain spectrum has a larger energy partitioning for the wavelengths of 1,000–5,000 nm (i.e., the 3rd–5th CLM bands; Figure S5 in Supporting Information S1) compared to the mid-latitude summer spectrum, where snow albedo is much lower at wavelengths of 1,000–5,000 nm than wavelengths of 700–1,000 nm and hence leads to lower overall NIR albedo values. The differences under diffuse radiation are much weaker (<0.01) due to smaller differences between the two spectra for diffuse radiation (Figure 6d and Figure S5 in Supporting Information S1). The impact is also very small in the visible band

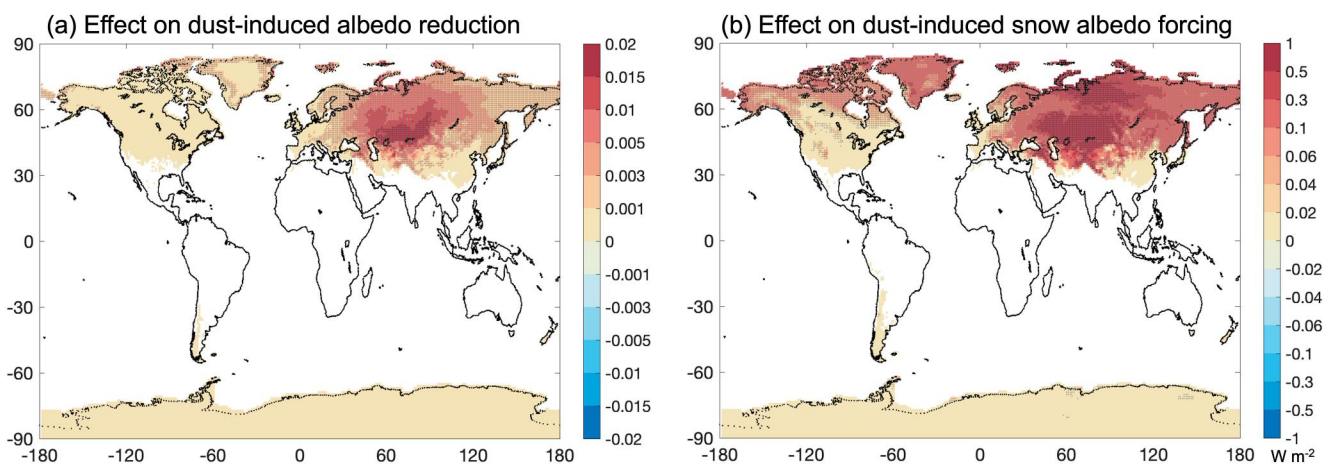

Figure 5. 5-year (2006–2010) all-sky annual mean effects of different dust types (i.e., differences between simulations using Greenland dust and Colorado dust): (a) difference for snow-covered (0%< snow cover ≤100%) ground albedo reduction caused by dust, (b) difference for dust-induced grid-mean snow albedo forcing (W m^{-2}). Regions with statistically significant differences ($p < 0.05$) are marked by gray "+" symbols.

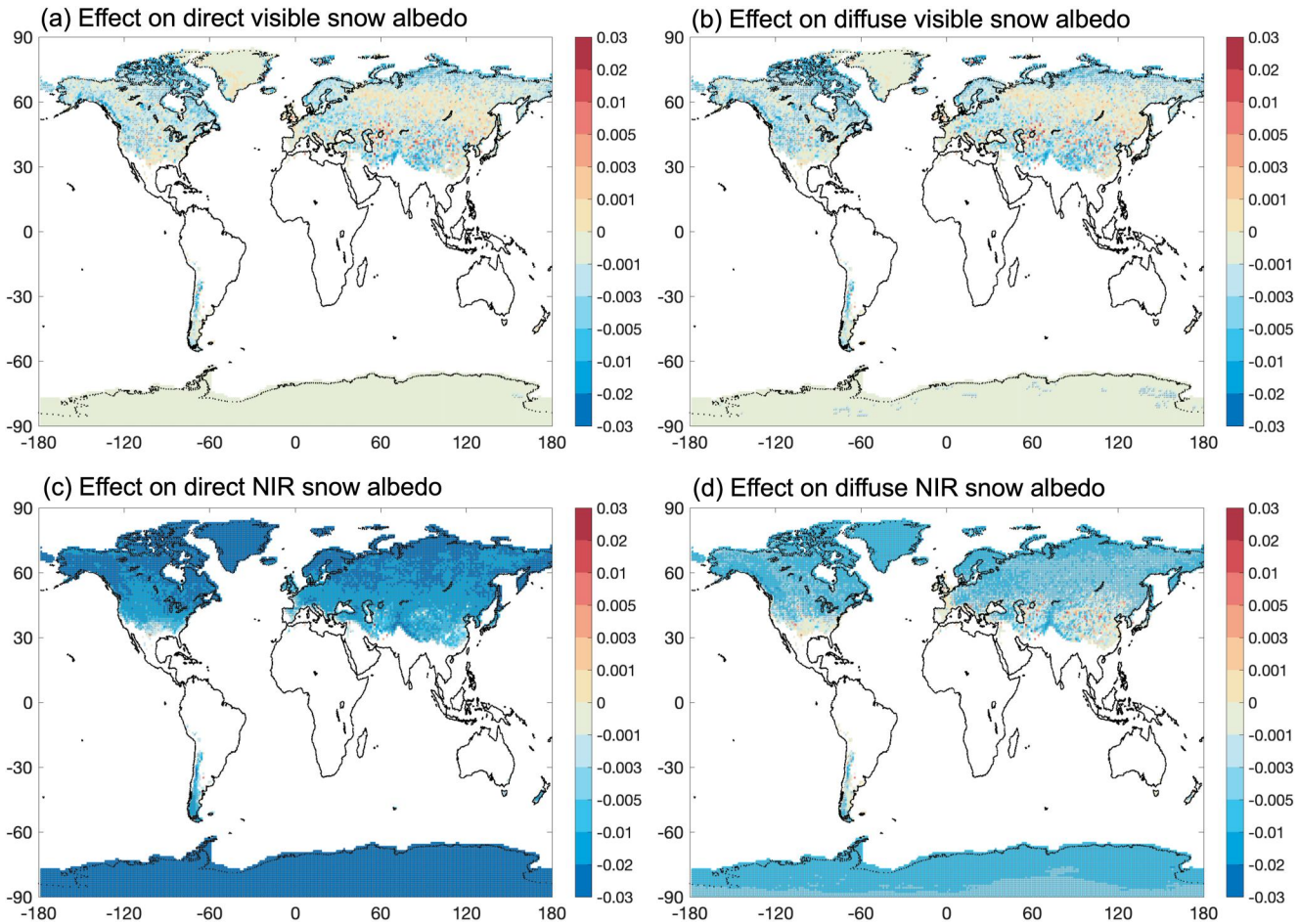

Figure 6. 5-year (2006–2010) annual mean effects of different downward solar spectra (i.e., differences between simulations using high mountain and mid-latitude summer spectra): (a) difference for direct-beam visible snow albedo, (b) difference for diffuse visible snow albedo, (c) difference for direct-beam NIR snow albedo, (d) difference for diffuse NIR snow albedo. Regions with statistically significant differences ($p < 0.05$) are marked by gray "+" symbols.

(Figures 6a and 6b), with some scattered but statistically insignificant differences in the northern mid-latitudes due to slight changes in other snow properties such as grain size, snow density, and/or snowpack thickness.

3.5. Effects of Updated Radiative Transfer Solver

Figure 7 shows the 5-year annual mean snow albedo difference between simulations using the adding-doubling and Toon et al. (1989) radiative transfer solvers. The differences are small (<0.01) for the visible band but are significant (up to 0.03) for the NIR band under both direct and diffuse radiation. Specifically, using the adding-doubling solver leads to higher NIR snow albedo under direct radiation particularly in high-latitudes with a mean difference of about 0.02 (Figure 7c), whereas it leads to a lower NIR snow albedo under diffuse radiation particularly in high-latitudes with a mean difference of about −0.02 (Figure 7d). Overall, the adding-doubling solver results in higher all-sky shortwave snow albedo by about 0.01 over high-latitudes (Table 2). The difference patterns are similar across all the seasons with relatively larger differences in winter and spring (Figure S6 in Supporting Information S1). These results are consistent with the findings of Dang et al. (2019), where the adding-doubling solver has a similarly high accuracy as the Toon et al. (1989) solver for the visible band but substantially reduces the NIR albedo underestimates at solar zenith angle >75° under direct radiation and the NIR albedo overestimates under diffuse radiation caused by the Toon et al. (1989) solver. Thus, using the adding-doubling solver results in higher accuracy in snow albedo calculations.

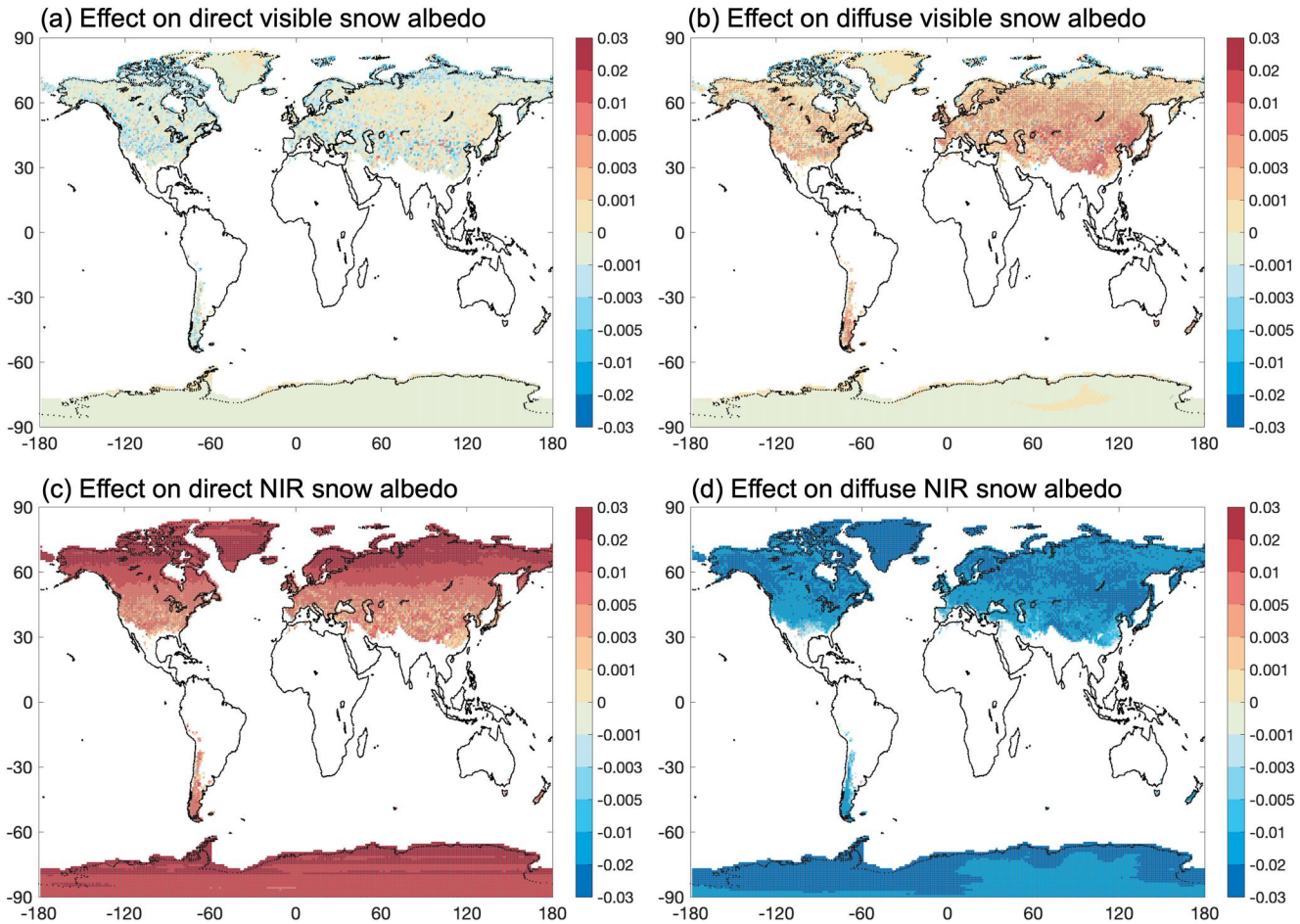

Figure 7. 5-year (2006–2010) annual mean effects of updated snow radiative transfer solvers (i.e., differences between simulations using the adding-doubling and Toon et al. (1989) solvers): (a) difference for direct-beam visible snow albedo, (b) difference for diffuse visible snow albedo, (c) difference for direct-beam NIR snow albedo, (d) difference for diffuse NIR snow albedo. Regions with statistically significant differences ($p < 0.05$) are marked by gray "+" symbols.

3.6. Effects of Nonspherical Snow Grains

Figure 8 shows the 5-year all-sky annual mean effects of nonspherical snow grains on snow albedo and aerosol-induced grid-mean snow albedo forcing by using fractal snowflakes versus snow spheres. These two grain shapes have the largest difference in snow optical properties, which demonstrates the upper limit of model sensitivity to snow nonsphericity in CLM5. Compared to using snow spheres, using fractal snowflakes leads to substantially higher snow albedo by more than 0.08 over some hotspots and by ∼0.04 over the global snowpack, with a stronger impact over northern mid-latitudes and two polar regions (Figure 8a and Table 2). Seasonally, the albedo increase due to the use of fractal snowflakes are consistently strong across all seasons (Figure S7 in Supporting Information S1). This is consistent with the conclusions from previous studies (Dang et al., 2016; Räisänen et al., 2017; He, Liou, et al., 2018), where nonspherical snow grains have lower asymmetry factor (i.e., weaker forward scattering) and hence higher snow albedo by 0.02–0.05 on average, depending on specific grain shape, grain size, and snow density and thickness.

In addition, previous studies (He, Liou, et al., 2018, 2019; Shi et al., 2022) also found that nonspherical snow grains can reduce aerosol-induced snow albedo forcing because of the reduced forward scattering and hence less aerosol absorption throughout the snowpack column. This is confirmed by the results in this study, where using fractal snowflakes shows lower grid-mean snow albedo forcing for BC, dust, and OC by up to 0.3 W m^{-2} over some hotspots and by 0.02–0.05 W m^{-2} averaged over northern mid- and high-latitude snowpack (Table 3 and Figures 8b–8d), compared to using snow spheres. The higher aerosol-induced snow albedo forcing in the case of fractal snowflakes over some mid-latitude thin snowpack is caused by the changes in other snow properties such

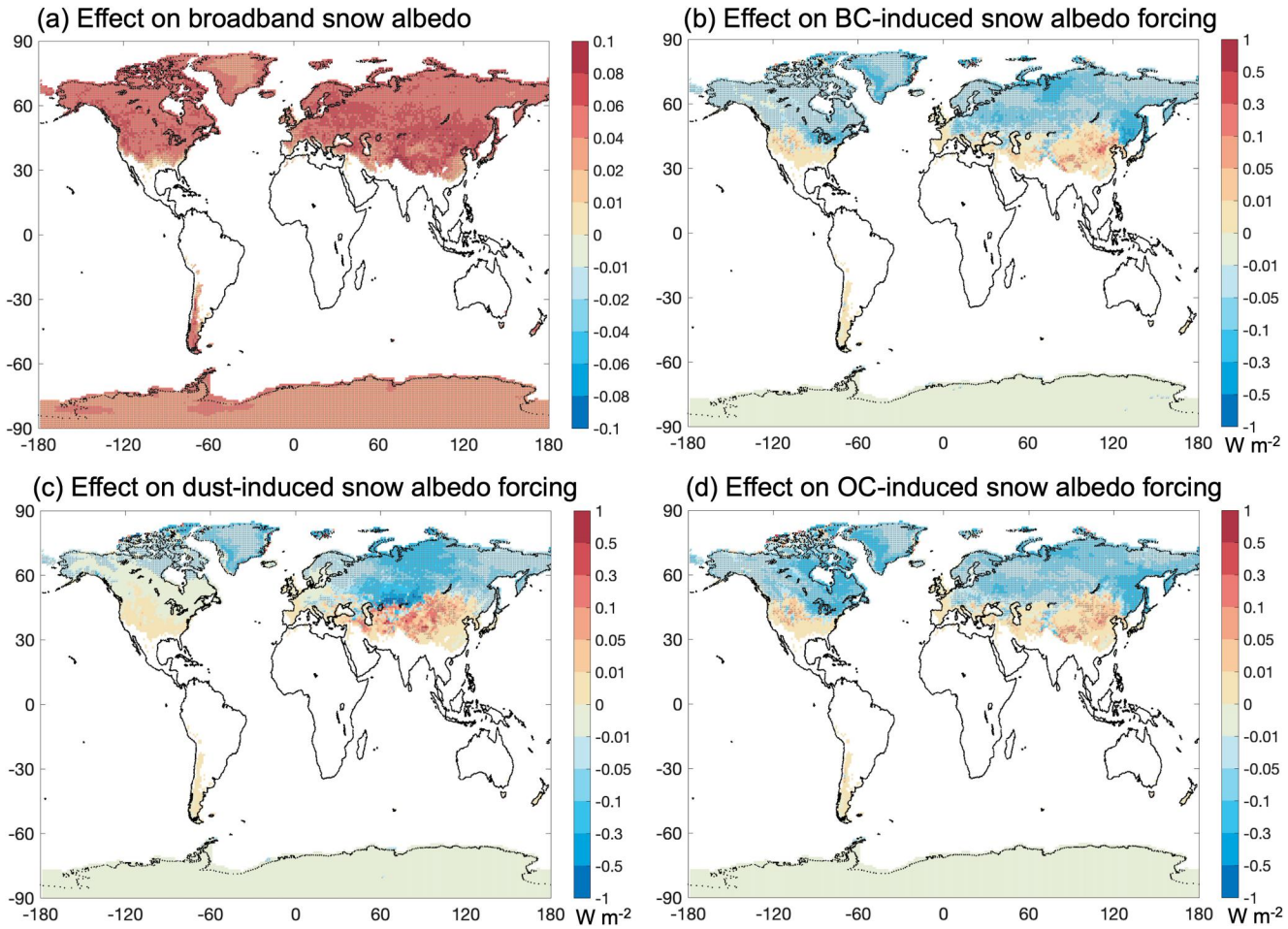

Figure 8. 5-year (2006–2010) all-sky annual mean effects of nonspherical snow grain (i.e., differences between simulations using fractal snowflake and snow sphere): (a) difference for broadband snow albedo, (b) difference for BC-induced grid-mean snow albedo forcing (W m^{-2}), (c) difference for dust-induced grid-mean snow albedo forcing (W m^{-2}), (d) difference for OC-induced grid-mean snow albedo forcing (W m^{-2}). Regions with statistically significant differences ($p < 0.05$) are marked by gray "+" symbols.

as snowpack thickness, grain size, and/or density, exceeding the direct impact of snow grain shape on aerosol light absorption in snowpack.

3.7. Effects of BC-Snow Internal Mixing

Figures 9a and 9b show the 5-year all-sky annual mean effects of BC-snow internal mixing on BC-induced snow-covered (0%< snow cover ≤100%) ground albedo reduction and albedo forcing, compared to external mixing. Overall, the internal mixing significantly enhances BC-induced snow albedo reduction by up to 0.05 and grid-mean albedo forcing by up to 5.0 W m^{-2} over heavily polluted snowpack, with an increase of 0.8–1.0 W m^{-2} in BC-induced snow albedo forcing averaged over northern mid- and high-latitude snowpack (Table 3) primarily during winter and spring (Figure S8 in Supporting Information S1). This is consistent with previous studies (Flanner et al., 2012; He, 2022), where the snow albedo reduction caused by internal mixing can be enhanced by up to 0.05 or more relative to external mixing, depending on snow grain size and shape, snowpack density and thickness, BC concentration in snow, and illumination conditions. He, Liou, et al. (2018) further found that the enhanced albedo reduction due to internal mixing increases the BC-induced snow albedo forcing by more than 1 W m^{-2} in polluted regions like northern China snowpack, which agrees with the results in this study. BC-snow internal mixing also reduces dust- and OC-induced snow albedo forcings by about 0.11 and 0.04 W m^{-2}, respectively, averaged over Northern Hemispheric snowpack (Table 3).

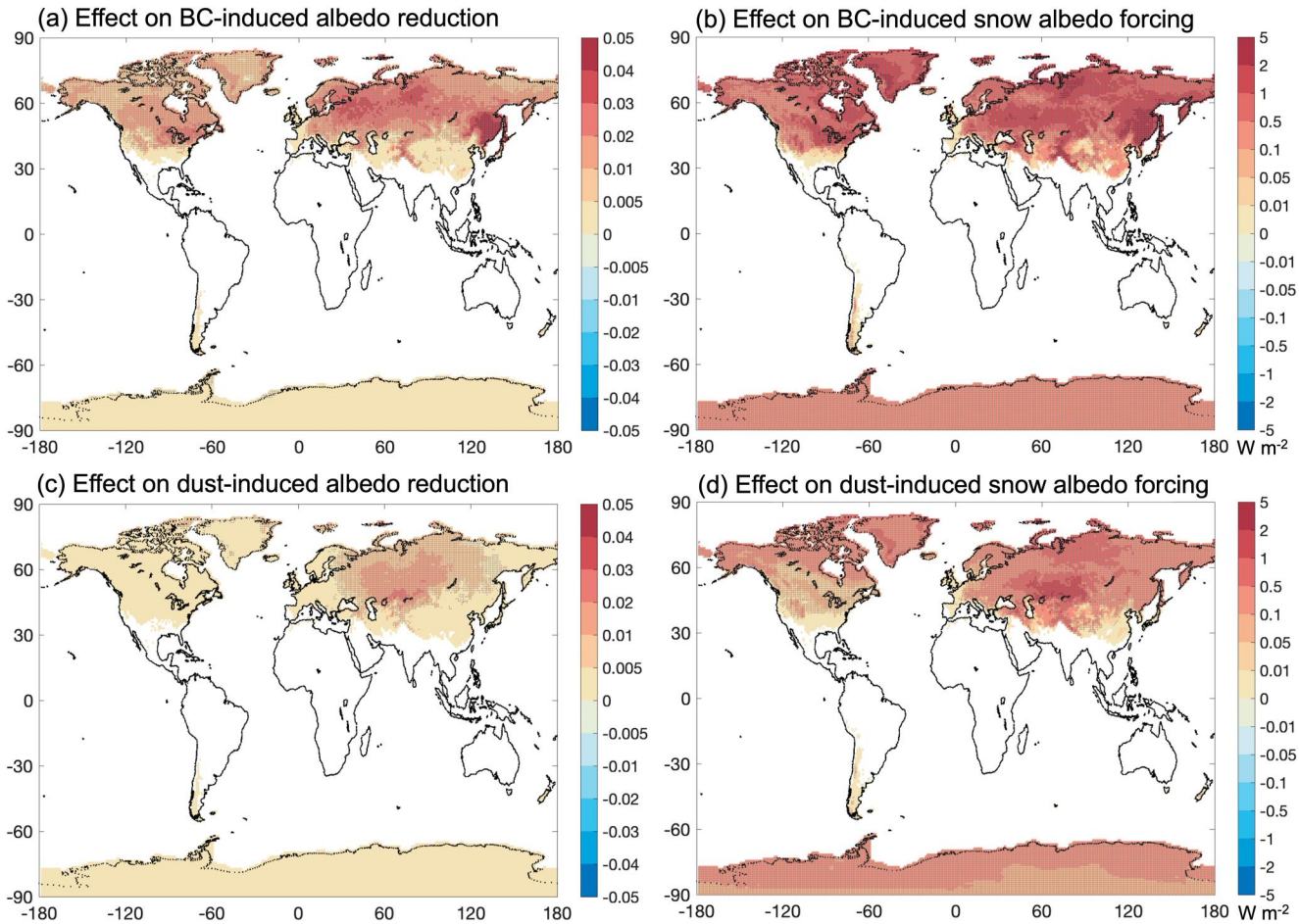

Figure 9. 5-year (2006–2010) all-sky annual mean effects of aerosol-snow internal mixing (i.e., differences between simulations using internal mixing and external mixing): (a) BC-snow internal mixing impact on BC-induced snow-covered (0%< snow cover ≤100%) ground albedo reduction, (b) BC-snow internal mixing impact on BC-induced grid-mean snow albedo forcing (W m^{-2}), (c) dust-snow internal mixing impact on dust-induced snow-covered (0%< snow cover ≤100%) ground albedo reduction, (b) dust-snow internal mixing impact on dust-induced grid-mean snow albedo forcing (W m^{-2}). Regions with statistically significant differences ($p < 0.05$) are marked by gray "+" symbols.

3.8. Effects of Dust-Snow Internal Mixing

Figures 9c and 9d show the 5-year all-sky annual mean effects of dust-snow internal mixing on dust-induced snow-covered (0%< snow cover ≤100%) ground albedo reduction and albedo forcing, compared to external mixing. Similar to BC-snow internal mixing, dust-snow internal mixing enhances snow albedo reduction by up to 0.03 and grid-mean albedo forcing by up to 2.0 W m^{-2} over heavily polluted snowpack, with an increase of 0.2–0.4 W m^{-2} in dust-induced snow albedo forcing averaged over northern mid- and high-latitude snowpack (Table 3) primarily in the northern Eurasia during winter and spring (Figures 9c–9d and Figure S9 in Supporting Information S1). This is consistent with previous findings (He, Liou, et al., 2019; Shi et al., 2021, 2022), where dust-snow internal mixing can result in 10%–45% enhancement in dust-induced snow albedo reduction and albedo forcing relative to external mixing, depending on snow grain size and shape, snowpack density and thickness, dust content in snow, and illumination conditions. Dust-snow internal mixing also slightly reduces BC- and OC-induced snow albedo forcing by about 0.025 and 0.045 W m^{-2}, respectively, averaged over Northern Hemispheric snowpack (Table 3).

3.9. Effects of New Hyperspectral Capability

Figure 10 shows the 5-year annual mean difference in snow albedo between simulations using hyperspectral (480-band) and 5-band calculations. The differences in visible snow albedo under direct and diffuse radiation are small

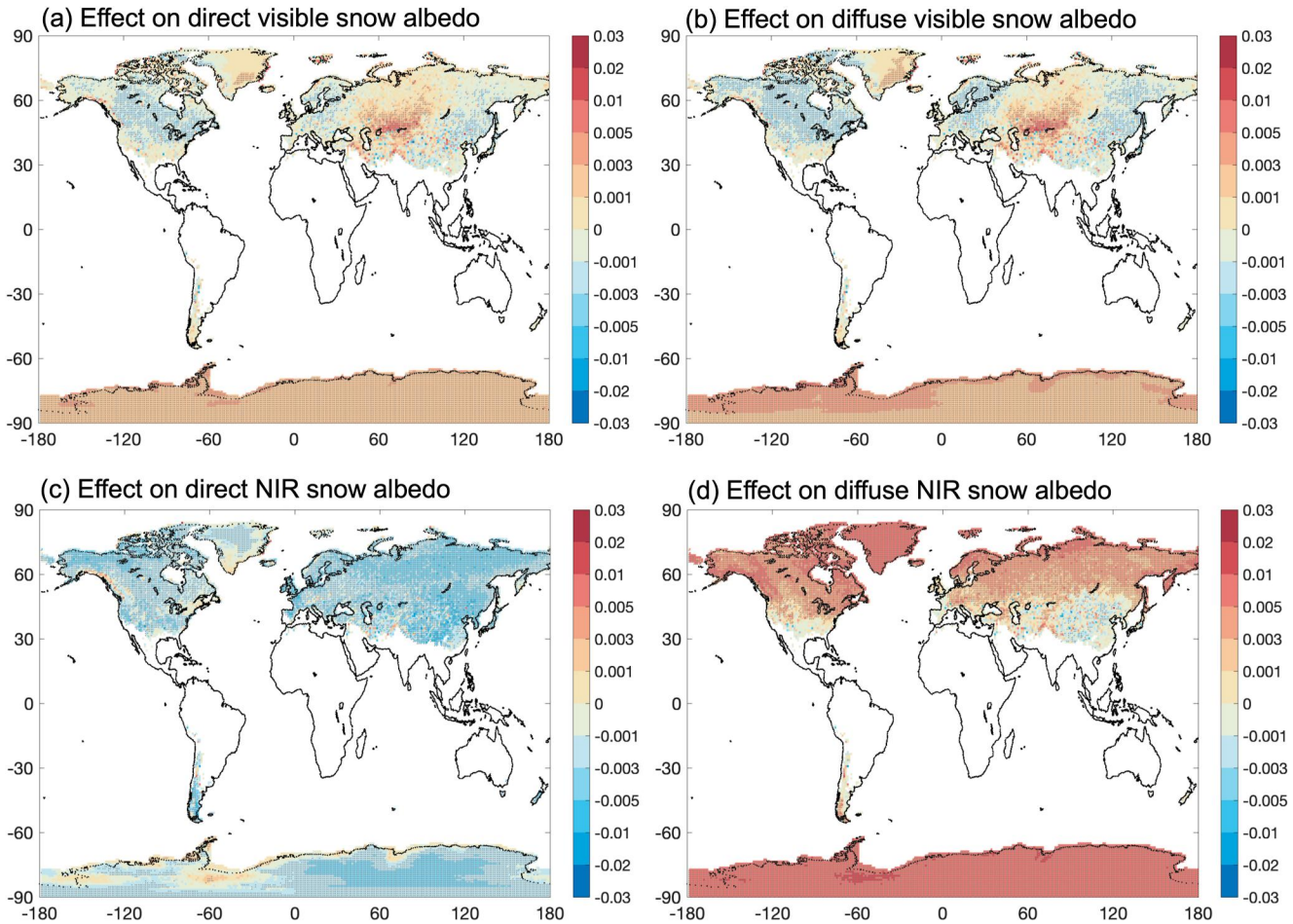

Figure 10. 5-year (2006–2010) annual mean effects of hyperspectral calculations (i.e., differences between simulations using 480 bands and 5 bands): (a) difference for direct-beam visible snow albedo, (b) difference for diffuse visible snow albedo, (c) difference for direct-beam NIR snow albedo, (d) difference for diffuse NIR snow albedo. Regions with statistically significant differences ($p < 0.05$) are marked by gray "+" symbols.

(<0.005), except for an increase of 0.005–0.01 using the 480-band calculation over the central Eurasian snowpack dominated by dust contamination (Figures 10a and 10b), where dust-induced snow albedo forcing is reduced by up to 0.3 W m^{-2} (Figure 11b). The 480-band calculation leads to widespread lower and higher NIR albedo under direct and diffuse radiation by about 0.01, respectively (Figures 10c and 10d), compared to the 5-band calculation. Overall, the 480-band calculation results in a slightly lower all-sky shortwave snow albedo by ∼0.001 averaged across different latitudinal snowpack (Table 2). In addition, the 480-band calculation also results in nontrivial differences in aerosol-induced grid-mean snow albedo forcing relative to the 5-band calculation (Figure 11 and Table 3), with higher BC forcing (by up to 0.20 W m^{-2} over northern China and Himalayas) and OC forcing (by up to 0.25 W m^{-2} over Northern Hemispheric hotspot areas) but lower dust forcing (by up to >0.3 W m^{-2} over the central Eurasia).

4. Model Evaluation

4.1. Surface Albedo

Figure 12 shows the comparison between MODIS observed and CLM5 simulated 5-year annual mean white-sky (diffuse) surface albedo over snow-covered (0%< snow cover ≤100%) regions. The default baseline simulation tends to overestimate the visible and NIR surface albedo in many parts of northern high- and mid-latitudes by about 0.1–0.2, but underestimates the albedo in the western US mountains, northern Middle East, northwestern Tibetan Plateau, and northern China by about 0.1 (Figures 12b and 12e). Compared to the default baseline result, the new baseline simulation with CLM5-SNICAR enhancements reduces the albedo underestimate in the western

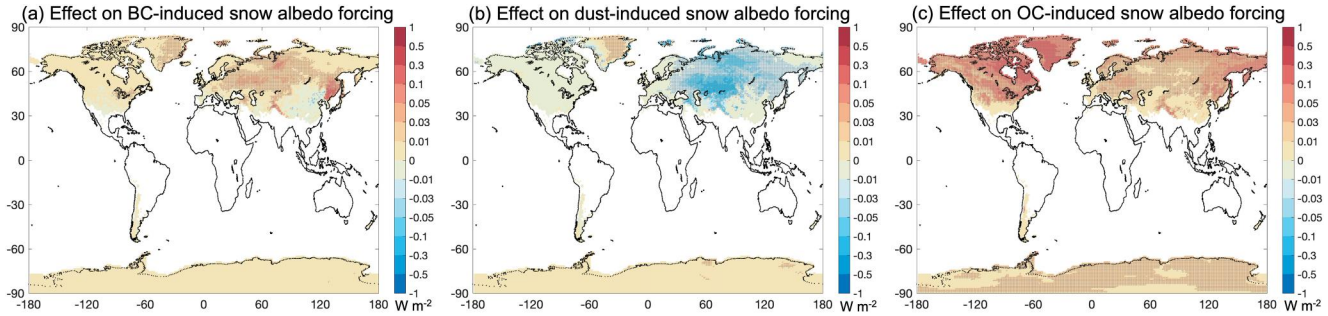

Figure 11. 5-year (2006–2010) all-sky annual mean effects of hyperspectral calculations (i.e., differences between simulations using 480 bands and 5 bands) on aerosol-induced grid-mean snow albedo forcing (W m^{-2}): (a) difference for BC, (b) difference for dust, (c) difference for OC. Regions with statistically significant differences ($p < 0.05$) are marked by gray "+" symbols.

US mountains, northern Middle East, northwestern Tibetan Plateau, and northern China by up to 0.1 for both visible and NIR bands (Figures 12c and 12f), primarily due to the use of nonspherical snow grains. The new baseline simulation also increases the snow-covered surface albedo in northern and southern high-latitudes by up to 0.1 mainly at the NIR band, which however exacerbates the model bias in high-latitudes. These patterns are generally consistent throughout different seasons (Figures S10 and S11 in Supporting Information S1). The assessment for black-sky snow-covered surface albedo shows similar results and conclusions (Figure S12 in Supporting Information S1). Overall, the new baseline simulation increases the model overestimates of surface albedo by about 0.01–0.03 averaged over different latitudinal bands (Table 4), although it reduces the bias in some northern mid-latitude regions mentioned above.

For the surface albedo underestimate in the default baseline simulation over the aforementioned mid-latitude regions, in addition to the bias in snow albedo calculations, it is also partially caused by model underestimates of snow cover (Section 4.2). The surface albedo overestimates in some mid-latitude regions, such as central

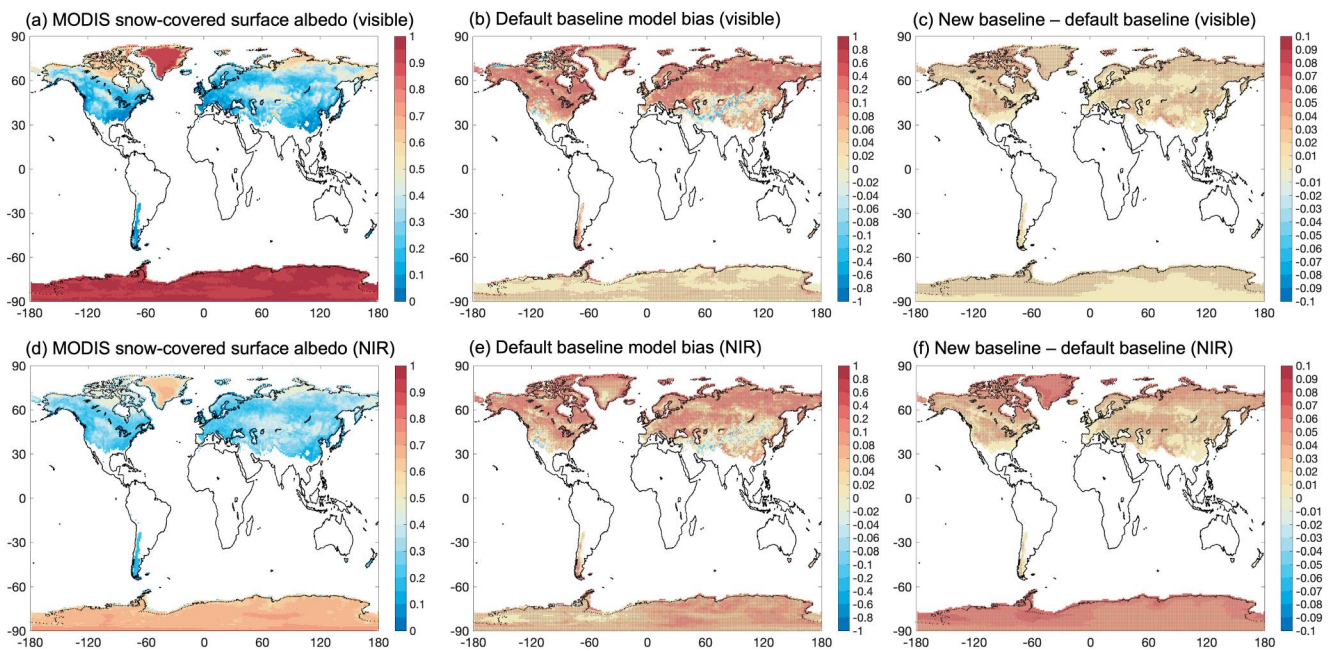

Figure 12. Comparison between MODIS and model simulations of 5-year (2006–2010) annual mean white-sky surface albedo over snow-covered (0%< snow cover ≤100%) regions. First column (a, d): MODIS observations; second column (b, e): default baseline simulation bias; third column (c, f): difference between new and default baseline simulations. First row (a, b, c): visible band; second row (d, e, f): NIR band. Regions with statistically significant differences ($p < 0.05$) are marked by gray "+" symbols.

Table 4
Summary of Model Evaluation Statistics

	Model annual mean biases[a]							
	Northern high-latitudes (90° N–60°N)		Northern mid-latitudes (60° N–30°N)		Southern mid-latitudes (30° S–60°S)		Southern high-latitudes (60° S–90°S)	
Land surface fields	Default baseline	New baseline	Default baseline	New baseline	Default baseline	New baseline	Default baseline	New baseline
Surface albedo (0%< snow cover ≤100%)	0.13	0.16	0.11	0.13	0.12	0.12	0.03	0.06
Snow cover	<0.01	0.01	−0.05	−0.04	−0.15	−0.15	<0.01	<0.01
SWE (mm) (seasonal snowpack)	13.6	16.5	−3.83	−2.77	−12.8	−12.6	–	–
Snow depth (mm) (seasonal snowpack)	−67.3	−60.3	−55.9	−53.0	−47.3	−46.9	–	–
2-m temperature (°C)	−0.54	−0.59	0.11	0.08	0.58	0.58	2.26	2.10

[a]All values in this table are statistically significant ($p < 0.05$).

Europe, southern Russia, northeastern US, and southern Canada, are partially due to the snow cover overestimates (Section 4.2). We note that the surface albedo overestimates in northern mid- and high-latitudes (except polar areas) primarily occur over forested regions and are likely a result of model uncertainties in vegetation characteristics (e.g., vegetation cover, canopy height, and LAI), canopy radiative transfer, and/or canopy interception of snow. Previous studies found that CLM5 surface albedo is sensitive to forest structures such as LAI and canopy height (Malle et al., 2021). The canopy intercepted snow is also not well constrained by observations. In addition, the uncertainty in CLM5 leaf optical properties were also found to affect surface albedo modeling (Dong et al., 2021).

The positive surface albedo bias over Greenland and Antarctica, which are mostly free of vegetation cover, can be most unambiguously related to the uncertainties in snow albedo calculations. A few factors could play a role. First, the modeled snow grain size may be underestimated due to too small grain size assumed for freshly fallen snow and/or too weak snow aging over Greenland and Antarctica. Second, the lack of BC- and dust-snow internal mixing effects may contribute to the positive albedo bias. Third, CLM5 does not account for the impact of snow surface roughness on snow albedo, which could lead to albedo overestimates particularly at NIR wavelengths (Larue et al., 2020; Manninen et al., 2021), consistent with our results (Figures 12b and 12e). Fourth, our parameterization of snow grain nonsphericity does not include the effect on snow single-scattering albedo due to its relatively small changes compared to asymmetry factor (Flanner et al., 2021). However, previous studies indicated that nonspherical snow particles with the same effective grain size exhibit slightly stronger absorption and hence lower single-scattering albedo than their spherical counterparts (Kokhanovsky & Zege, 2004; Libois et al., 2014; Räisänen et al., 2017; Robledano et al., 2023), which may contribute to the positive albedo bias in our new baseline simulations.

We note that it is likely that the reduced albedo bias by using the new baseline scheme over some areas might mask biases that are related to snowpack processes other than snow albedo calculations. This issue, however, is outside the scope of this study. We also note that the MODIS surface albedo product has uncertainties (see Section 4.6), which may affect the model evaluation results.

4.2. Snow Cover

Figure 13 and Figure S13 in Supporting Information S1 shows the comparison between MODIS observed and CLM5 simulated 5-year annual and seasonal mean snow cover fraction, respectively. The default baseline simulation significantly underestimates snow cover in the Tibetan Plateau, North American Rocky Mountains, northern Middle East, northwestern China, and southern Andes throughout the year by about 0.25, whereas the new baseline simulation reduces the bias by up to 0.1 in these regions (Figure 13b and Figure S13 in Supporting Information S1). This is primarily caused by the increased surface albedo over those regions in the new baseline simulation (Section 4.1), which reduces the solar radiation absorbed by snowpack and hence increases snow cover. The default baseline simulation overestimates snow cover by 0.1–0.2 in the northeastern US, southern

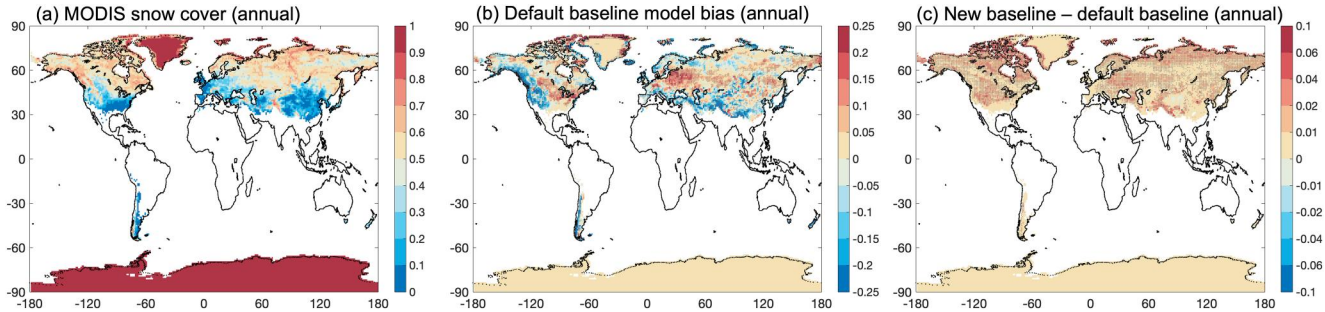

Figure 13. Comparison between MODIS and model simulations of 5-year (2006–2010) annual mean snow cover fraction: (a) MODIS observations, (b) default baseline simulation bias, (c) difference between new and default baseline simulations. See Figure S13 in Supporting Information S1 for seasonal results. Regions with statistically significant differences ($p < 0.05$) are marked by gray "+" symbols.

Canada, central Europe, northeastern China, and southern Russia, whereas the new baseline simulation slightly exacerbates the bias by ~0.02. Overall, the new baseline simulation reduces the mean snow cover biases in the northern and southern mid-latitudes, but increases the bias in northern high-latitudes (Table 4 and Table S1 in Supporting Information S1).

4.3. Snow Water Equivalent

Figure 14 and Figure S14 in Supporting Information S1 shows the comparison between ERA5-Land and CLM5 simulated 5-year annual and seasonal mean snow water equivalent (SWE) over seasonal snowpack, respectively. We note that the SWE and snow depth over permanent snowpack in glaciers and mountains are sensitive to model assumptions and initialization used in the ERA5-Land data set and CLM5, which cannot reveal typical SWE and snow depth biases in the CLM5 simulation. Also, the maximum SWE allowed (i.e., SWE capping) in the CLM5 is set to 10,000 kg/m^2 to prevent unlimited snow building up over glacier regions in model simulations (particularly a coupled climate run), which would cause serious model issues (e.g., incorrect land water storage and ocean salinity). Thus, when evaluating simulated SWE and snow depth (see Section 4.4), we only included the regions with seasonal snowpack (i.e., zero yearly minimum SWE).

The default baseline simulation underestimates SWE by up to 50 mm in the northwestern and southeastern Tibetan Plateau, North American Rocky Mountains, southern Russia, northern Middle East, and southern Andes across most seasons (Figure 14 and Figure S14 in Supporting Information S1). Compared to the default baseline result, the new baseline simulation increases SWE and hence reduces the bias by up to 20 mm in the aforementioned regions (Figure 14 and Figure S14 in Supporting Information S1). This is because the increased surface albedo over those regions in the new baseline simulation (Section 4.1) reduces snow melting and hence increases SWE. The default baseline simulation overestimates SWE in northern Eurasia and northeast US/southeast Canada, likely due to the precipitation bias, uncertainties in snow interception by canopy, and/or underestimated snow ablation caused by the positive surface albedo bias in these regions (Figure 12b). Overall, the new baseline simulation reduces the mean SWE biases (underestimates) in northern and southern

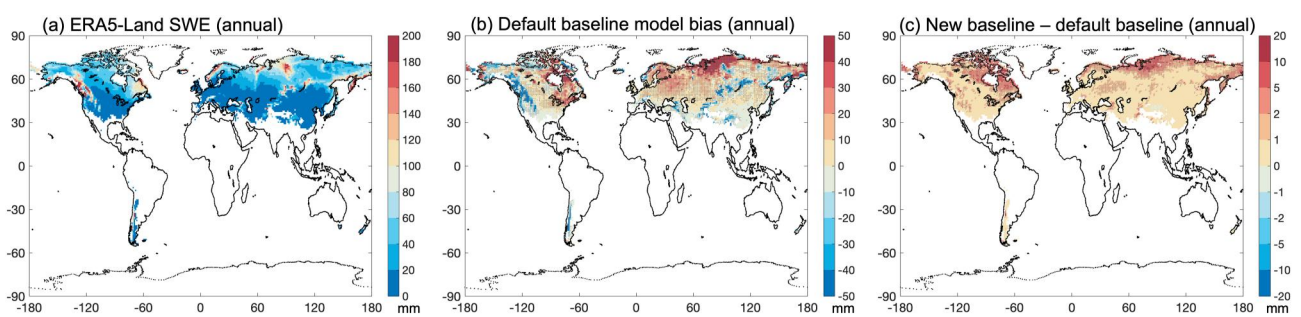

Figure 14. Comparison between ERA5-Land and model simulations of 5-year (2006–2010) annual mean SWE (mm) over seasonal snowpack only: (a) ERA5-Land data, (b) default baseline simulation bias, (c) difference between new and default baseline simulations. See Figure S14 in Supporting Information S1 for seasonal results. Regions with statistically significant differences ($p < 0.05$) are marked by gray "+" symbols.

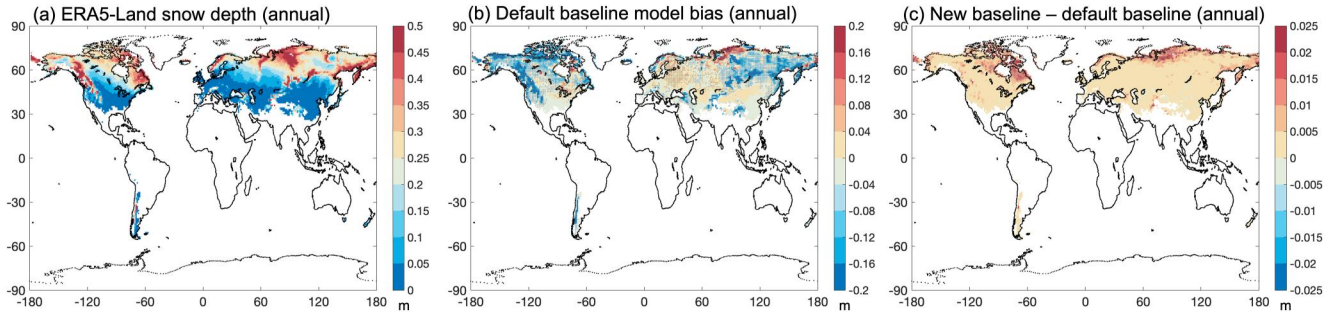

Figure 15. Same as Figure 14, but for snow depth (m) comparison between ERA5-Land and model simulations. See Figure S15 in Supporting Information S1 for seasonal results. Regions with statistically significant differences ($p < 0.05$) are marked by gray "+" symbols.

mid-latitudes, but exacerbates the overestimates in northern high-latitudes (Table 4 and Table S1 in Supporting Information S1).

4.4. Snow Depth

Figure 15 and Figure S15 in Supporting Information S1 shows the comparison between ERA5-Land and CLM5 simulated 5-year annual and seasonal mean snow depth, respectively. Similar to the SWE evaluation (Section 4.3), we only included the regions with seasonal snowpack. The default baseline simulation underestimates snow depth by up to 0.2 m over most of the global seasonal snowpack except for Europe, part of northern Russia, and East Asia. Compared to the default baseline result, the new baseline simulation reduces the snow depth bias by 0.02 m over the northwestern Tibetan Plateau, North American Rocky Mountains, northern Canada, and southern Andes (Figure 15 and Figure S15 in Supporting Information S1). This is caused by the less light absorption by snowpack over those regions in the new baseline simulation (Section 4.1), which weakens snow densification/melting and hence increases snow depth. The new baseline simulation, however, exacerbates the snow depth overestimates by 0.02 m over part of northern Russia. Overall, the new baseline simulation reduces the mean snow depth biases (underestimates) over the seasonal snowpack across different latitudinal bands (Table 4 and Table S1 in Supporting Information S1).

4.5. 2-m Surface Air Temperature

Figure 16 and Figure S16 in Supporting Information S1 shows the comparison between ERA5-Land and CLM5 simulated 5-year annual and seasonal mean surface (2-m) air temperature, respectively. The default baseline simulation generally overestimates the 2-m air temperature by up to 5°C over the snowpack in the southern Greenland, the Tibetan Plateau, the Andes, and most parts of Antarctica throughout the year, and underestimates in western Russia, northern Canada, and northern Greenland. Compared to the default baseline result, the new baseline simulation reduces the 2-m air temperature overestimates by up to 0.25°C over the Antarctica, southern Greenland, western and southern Tibetan Plateau, and western US mountains (Figure 16 and Figure S16 in Supporting Information S1). This is because of the increased surface albedo and hence less surface heating by solar radiation absorption over those regions in the new baseline simulation (Section 4.1). The new baseline simulation, however, tends to slightly worsen the model temperature bias in the western Russia and northern Canada. Overall, the new baseline simulation reduces the mean 2-m surface air temperature biases (overestimates) across different latitudinal bands except for northern high-latitudes (Table 4 and Table S1 in Supporting Information S1). The impact on 2-m air temperature, which is strongly constrained by the forcing temperature in land-only simulations, is expected to be stronger in a coupled climate simulation through positive surface albedo feedbacks.

4.6. Uncertainty Discussions

We note that the MODIS and ERA5-Land data sets used for the model evaluations in Sections 4.1–4.5 also have uncertainties. For example, the MODIS surface albedo retrievals are influenced by cloud conditions and solar zenith angle, with 3.5% and 5.5% errors for visible and NIR bands, respectively, at a nadir solar zenith angle under clear sky conditions (Schaaf & Wang, 2021). The errors increase up to 10% at non-nadir solar zenith angle under

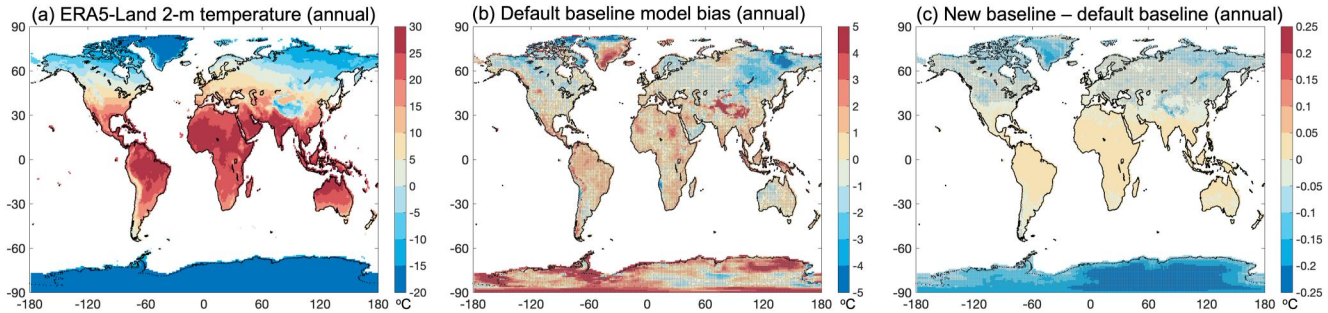

Figure 16. Comparison between ERA5-Land and model simulations of 5-year (2006–2010) annual mean 2-m air temperature (°C): (a) ERA5-Land data, (b) default baseline simulation bias, and (c) difference between new and default baseline simulations. Regions with statistically significant differences ($p < 0.05$) are marked by gray "+" symbols.

cloudy conditions. The MODIS snow cover retrievals are affected by both clouds and forests, with relatively lower accuracy over cloudy conditions and forested regions. Previous studies have reported an overall accuracy of 88%–93% for MODIS snow cover products (Hall and Riggs, 2021a, 2021b). To achieve a balance between sufficient samples and data quality, we have selected MODIS snow cover data with quality of "good" or better with less than 20% cloud fraction. For ERA5-Land, although it assimilates many satellite and in situ observations into the product, it still heavily relies on the accuracy of its modeling system. Previous studies have shown that ERA5-Land snow data are generally consistent with other reanalysis products (Mortimer et al., 2020), but tend to overestimate SWE and slightly underestimate very deep snowpack during late snow seasons (Lei et al., 2023; Mortimer et al., 2020). For snow quantities that have no spatiotemporally continuous global high-accuracy satellite observations, the ERA5-Land reanalysis still serves as an important reference data set for model comparison.

5. Conclusions

In this study, we enhanced the CLM5-SNICAR snow albedo modeling by implementing several new features with more realistic and physical representations of snow-aerosol-radiation interactions. Specifically, we incorporated the following model enhancements: (a) updating ice and aerosol optical properties with more realistic and accurate data sets; (b) adding multiple dust types; (c) adding multiple surface downward solar spectra to account for different atmospheric conditions; (d) incorporating a more accurate adding-doubling radiative transfer solver; (e) adding nonspherical snow grain representation; (f) adding BC-snow and dust-snow internal mixing representations; (g) adding a hyperspectral (480-band vs. the default 5-band) modeling capability. These model features/enhancements have been included as new CLM physics/namelist options, which allows for quantifying model sensitivities to snow albedo processes and for conducting relevant multi-physics model ensemble analyses for uncertainty assessment. The model updates have been included in the latest released CLM version. Sensitivity analyses revealed strong impacts of using the new adding-doubling solver, nonspherical snow grains, aerosol-snow internal mixing, updated aerosol optics, and different dust types.

The enhanced snow albedo representations improve the CLM5 modeled snowpack evolution and land surface conditions in many parts of the globe. Specifically, the enhanced CLM5-SNICAR leads to (a) a reduced snow-covered surface albedo bias (underestimate) in several key northern mid-latitude regions, including western US mountains, northern Middle East, northwestern Tibetan Plateau, and northern China, but a generally increased bias when averaged over different latitudinal bands; (b) a reduced snow cover bias (underestimate) in northern and southern mid-latitudes, including the Tibetan Plateau, North American Rocky Mountains, northern Middle East, northwestern China, and southern Andes, but a degraded mean performance in northern high-latitudes; (c) a reduced SWE bias (underestimate) in the mid-latitude seasonal snowpack, including northwestern and southeastern Tibetan Plateau, North American Rocky Mountains, southern Russia, northern Middle East, and southern Andes, but an exacerbated overestimate in northern high-latitudes; (d) a reduced snow depth bias (underestimate) in seasonal snowpack over regions like the northwestern Tibetan Plateau, North American Rocky Mountains, northern Canada, and southern Andes, but a worsened performance in part of northern Russia; (e) a reduced surface (2-m) air temperature bias (overestimate) over the Antarctica, southern Greenland, western and southern Tibetan Plateau, and western US mountains, but a degradation in the western Russia and northern Canada.

In future studies, other snowpack processes and coupled climate model simulations with the enhanced CLM5-SNICAR will need to be assessed and improved to quantify the full climatic impacts of the snow albedo enhancements added in this study, which are expected to be stronger than those shown here due to positive snow albedo feedback.

Conflict of Interest

The authors declare no conflicts of interest relevant to this study.

Data Availability Statement

The CLM5-SNICAR code is from CTSM Development Team (2022). MODIS surface albedo data (MCD43C3) is from Schaaf and Wang (2021). MODIS snow cover data (MOD10C1 and MYD10C1) is from Hall and Riggs (2021a, 2021b), respectively. ERA5-Land data (SWE, snow depth, surface temperature) is from Muñoz Sabater (2019). The model data generated in this study can be obtained in He et al. (2023).

Acknowledgments
The authors thank the reviewers and editor for their constructive comments, which substantially improve the paper quality. This research was funded by the U.S. National Oceanic and Atmospheric Administration (NOAA) Climate Process Team project Award# 4000178550 and Award# NA19OAR4310243. NSF NCAR is sponsored by the U.S. National Science Foundation. Any opinions, findings, conclusions, or recommendations expressed in this publication are those of the authors and do not necessarily reflect the views of the National Science Foundation.

References

Abolafia-Rosenzweig, R., He, C., McKenzie Skiles, S., Chen, F., & Gochis, D. (2022). Evaluation and optimization of snow albedo scheme in Noah-MP land surface model using in situ spectral observations in the Colorado Rockies. *Journal of Advances in Modeling Earth Systems*, *14*(10), e2022MS003141. https://doi.org/10.1029/2022MS003141

Bales, R. C., Molotch, N. P., Painter, T. H., Dettinger, M. D., Rice, R., & Dozier, J. (2006). Mountain hydrology of the western United States. *Water Resources Research*, *42*(8), 1–13. https://doi.org/10.1029/2005WR004387

Briegleb, B. P., & Light, B. (2007). A delta-eddington multiple scattering parameterization for solar radiation in the sea ice component of the community climate system Model. NCAR Tech. Note 472 1 STR (p. 100).

Chen, F., Barlage, M., Tewari, M., Rasmussen, R., Jin, J., Lettenmaier, D., et al. (2014). Modeling seasonal snowpack evolution in the complex terrain and forested Colorado Headwaters region: A model intercomparison study. *Journal of Geophysical Research: Atmospheres*, *119*(24), 13795–13819. https://doi.org/10.1002/2014JD022167

Cook, J. M., Hodson, A. J., Gardner, A. S., Flanner, M., Tedstone, A. J., Williamson, C., et al. (2017). Quantifying bioalbedo: A new physically based model and discussion of empirical methods for characterising biological influence on ice and snow albedo. *The Cryosphere*, *11*(6), 2611–2632. https://doi.org/10.5194/tc-11-2611-2017

CTSM Development Team. (2022). ESCOMP/CTSM: NEON release: Some NEON updates fixing AG sites, update MOSART, small fixes (ctsm5.1.dev114) [Software]. Zenodo. https://doi.org/10.5281/zenodo.7342803

Danabasoglu, G., Lamarque, J. F., Bacmeister, J., Bailey, D. A., DuVivier, A. K., Edwards, J., et al. (2020). The community Earth system model version 2 (CESM2). *Journal of Advances in Modeling Earth Systems*, *12*. https://doi.org/10.1029/2019MS001916

Dang, C., Brandt, R. E., & Warren, S. G. (2015). Parameterizations for narrowband and broadband albedo of pure snow and snow containing mineral dust and black carbon. *Journal of Geophysical Research: Atmospheres*, *120*(11), 5446–5468. https://doi.org/10.1002/2014JD022646

Dang, C., Fu, Q., & Warren, S. G. (2016). Effect of snow grain shape on snow albedo. *Journal of the Atmospheric Sciences*, *73*(9), 3573–3583. https://doi.org/10.1175/JAS-D-15-0276.1

Dang, C., Zender, C. S., & Flanner, M. G. (2019). Intercomparison and improvement of two-stream shortwave radiative transfer schemes in Earth system models for a unified treatment of cryospheric surfaces. *The Cryosphere*, *13*(9), 2325–2343. https://doi.org/10.5194/tc-13-2325-2019

Dirmeyer, P. A., Gao, X., Zhao, M., Guo, Z., Oki, T., & Hanasaki, N. (2006). GSWP-2: Multimodel analysis and implications for our per-ception of the land surface. *Bulletin America Meteorology Social*, *87*(10), 1381–1398. https://doi.org/10.1175/bams-87-10-1381

Dominé, F., Lauzier, T., Cabanes, A., Legagneux, L., Kuhs, W. F., Techmer, K., & Heinrichs, T. (2003). Snow metamorphism as revealed by scanning electron microscopy. *Microscopy Research and Technique*, *62*(1), 33–48. https://doi.org/10.1002/jemt.10384

Dong, W., Yuan, H., Zhang, R., Li, H., Huang, L., Zhu, S., et al. (2021). Effects of incorporating measured leaf optical properties in land surface models. *Frontiers of Earth Science*, *9*, 663917. https://doi.org/10.3389/feart.2021.663917

Dumont, M., Flin, F., Malinka, A., Brissaud, O., Hagenmuller, P., Lapalus, P., et al. (2021). Experimental and model-based investigation of the links between snow bidirectional reflectance and snow microstructure. *The Cryosphere*, *15*(8), 3921–3948. https://doi.org/10.5194/tc-15-3921-2021

Dumont, M., Tuzet, F., Gascoin, S., Picard, G., Kutuzov, S., Lafaysse, M., et al. (2020). Accelerated snow melt in the Russian Caucasus mountains after the Saharan dust outbreak in March 2018. *Journal of Geophysical Research: Earth Surface*, *125*(9), e2020JF005641. https://doi.org/10.1029/2020jf005641

Erbe, E. F., Rango, A., Foster, J., Josberger, E. G., Pooley, C., & Wergin, W. (2003). Collecting, shipping, storing, and imaging snow crystals and ice grains with low-temperature scanning electron microscopy. *Microscopy Research and Technique*, *62*(1), 19–32. https://doi.org/10.1002/jemt.10383

Essery, R., Rutter, N., Pomeroy, J., Baxter, R., Stahli, M., Gustafsson, D., et al. (2009). SNPWMIP2, an evaluation of froest snow process simulations. *Bulletin of the American Meteorological Society*, *90*, 1120–1135.

Flanner, M. G., Arnheim, J. B., Cook, J. M., Dang, C., He, C., Huang, X., et al. (2021). SNICAR-ADv3: A community tool for modeling spectral snow albedo. *Geoscientific Model Development*, *14*(12), 7673–7704. https://doi.org/10.5194/gmd-14-7673-2021

Flanner, M. G., Gardner, A. S., Eckhardt, S., Stohl, A., & Perket, J. (2014). Aerosol radiative forcing from the 2010 Eyjafjallajökull volcanic eruptions. *Journal of Geophysical Research: Atmospheres*, *119*(15), 9481–9491. https://doi.org/10.1002/2014jd021977

Flanner, M. G., Liu, X., Zhou, C., Penner, J. E., & Jiao, C. (2012). Enhanced solar energy absorption by internally-mixed black carbon in snow grains. *Atmospheric Chemistry and Physics*, *12*(10), 4699–4721. https://doi.org/10.5194/acp-12-4699-2012

Flanner, M. G., Shell, K. M., Barlage, M., Perovich, D. K., & Tschudi, M. A. (2011). Radiative forcing and albedo feedback from the Northern Hemisphere cryosphere between 1979 and 2008. *Nature Geoscience*, *4*(3), 151–155. https://doi.org/10.1038/ngeo1062

Flanner, M. G., Zender, C. S., Randerson, J. T., & Rasch, P. J. (2007). Present-day climate forcing and response from black carbon in snow. *Journal of Geophysical Research*, *112*(D11). https://doi.org/10.1029/2006jd008003

Gardner, A. S., & Sharp, M. J. (2010). A review of snow and ice albedo and the development of a new physically based broadband albedo parameterization. *Journal of Geophysical Research*, *115*(F1), F01009. https://doi.org/10.1029/2009JF001444

Gelman Constantin, J., Ruiz, L., Villarosa, G., Outes, V., Bajano, F. N., He, C., et al. (2020). Measurements and modeling of snow albedo at Alerce Glacier, Argentina: Effects of volcanic ash, snow grain size, and cloudiness. *The Cryosphere*, *14*(12), 4581–4601. https://doi.org/10.5194/tc-14-4581-2020

Gleason, K. E., McConnell, J. R., Arienzo, M. M., Chellman, N., & Calvin, W. M. (2019). Four-fold increase in solar forcing on snow in western US burned forests since 1999. *Nature Communications*, *10*(1), 2026. https://doi.org/10.1038/s41467-019-09935-y

Golaz, J. C., Caldwell, P. M., Van Roekel, L. P., Petersen, M. R., Tang, Q., Wolfe, J. D., et al. (2019). The DOE E3SM coupled model version 1: Overview and evaluation at standard resolution. *Journal of Advances in Modeling Earth Systems*, *11*(7), 2089–2129. https://doi.org/10.1029/2018ms001603

Gul, C., Mahapatra, P. S., Kang, S., Singh, P. K., Wu, X., He, C., et al. (2021). Black carbon concentration in the central Himalayas: Impact on glacier melt and potential source contribution. *Environmental Pollution*, *275*, 116544. https://doi.org/10.1016/j.envpol.2021.116544

Hall, D. K., & Riggs, G. A. (2021a). MODIS/Terra Snow Cover Daily L3 Global 0.05Deg CMG, Version 61 [Dataset]. Boulder, Colorado USA. NASA National Snow and Ice Data Center Distributed Active Archive Center. https://doi.org/10.5067/MODIS/MOD10C1.061

Hall, D. K., & Riggs, G. A. (2021b). MODIS/Aqua Snow Cover Daily L3 Global 0.05Deg CMG, Version 61 [Dataset]. Boulder, Colorado USA. NASA National Snow and Ice Data Center Distributed Active Archive Center. https://doi.org/10.5067/MODIS/MYD10C1.061

Hao, D., Bisht, G., Rittger, K., Bair, E., He, C., Huang, H., et al. (2023). Improving snow albedo modeling in the E3SM land model (version 2.0) and assessing its impacts on snow and surface fluxes over the Tibetan Plateau. *Geoscientific Model Development*, *16*(1), 75–94. https://doi.org/10.5194/gmd-16-75-2023

He, C. (2022). Modeling light-absorbing particle-snow-radiation interactions and impacts on snow albedo: Fundamentals, recent advances, and future directions. *Environmental Chemistry*, *19*(5), 296–311. https://doi.org/10.1071/EN22013

He, C., Chen, F., Abolafia-Rosenzweig, R., Ikeda, K., Liu, C., & Rasmussen, R. (2021). What causes the unobserved early-spring snowpack ablation in convection-permitting WRF modeling over Utah Mountains? *Journal of Geophysical Research: Atmospheres*, *126*(22), e2021JD035284. https://doi.org/10.1029/2021JD035284

He, C., Chen, F., Barlage, M., Liu, C., Newman, A., Tang, W., et al. (2019). Can convection-permitting modeling provide decent precipitation for offline high-resolution snowpack simulations over mountains? *Journal of Geophysical Research: Atmospheres*, *124*(23), 12631–12654. https://doi.org/10.1029/2019JD030823

He, C., & Flanner, M. (2020). Snow albedo and radiative transfer: Theory, modeling, and parameterization. In *Springer series in light scattering* (pp. 67–133). Springer.

He, C., Flanner, M., Lawrence, D., & Gu, Y. (2023). Model dataset for the journal publication entitled "new features and enhancements in community land model (CLM5) snow albedo modeling: Description, sensitivity, and evaluation" [Dataset]. Zenodo. https://doi.org/10.5281/zenodo.7986830

He, C., Flanner, M. G., Chen, F., Barlage, M., Liou, K. N., Kang, S., et al. (2018). Black carbon-induced snow albedo reduction over the Tibetan plateau: Uncertainties from snow grain shape and aerosol–snow mixing state based on an updated SNICAR model. *Atmospheric Chemistry and Physics*, *18*(15), 11507–11527. https://doi.org/10.5194/acp-18-11507-2018

He, C., Li, Q., Liou, K.-N., Takano, Y., Gu, Y., Qi, L., et al. (2014). Black carbon radiative forcing over the Tibetan Plateau. *Geophysical Research Letters*, *41*(22), 7806–7813. https://doi.org/10.1002/2014GL062191

He, C., Liou, K. N., & Takano, Y. (2018). Resolving size distribution of black carbon internally mixed with snow: Impact on snow optical properties and albedo. *Geophysical Research Letters*, *45*(6), 2697–2705. https://doi.org/10.1002/2018gl077062

He, C., Liou, K. N., Takano, Y., Chen, F., & Barlage, M. (2019). Enhanced snow absorption and albedo reduction by dust-snow internal mixing: Modeling and parameterization. *Journal of Advances in Modeling Earth Systems*, *11*(11), 3755–3776. https://doi.org/10.1029/2019ms001737

He, C., Liou, K. N., Takano, Y., Yang, P., Qi, L., & Chen, F. (2018). Impact of grain shape and multiple black carbon internal mixing on snow albedo: Parameterization and radiative effect analysis. *J. Geophys. Res.-Atmos.*, *123*(2), 1253–1268. https://doi.org/10.1002/2017jd027752

He, C., Takano, Y., & Liou, K. N. (2017). Close packing effects on clean and dirty snow albedo and associated climatic implications. *Geophysical Research Letters*, *44*(8), 3719–3727. https://doi.org/10.1002/2017gl072916

He, C., Takano, Y., Liou, K. N., Yang, P., Li, Q., & Chen, F. (2017). Impact of snow grain shape and black carbon–snow internal mixing on snow optical properties: Parameterizations for climate models. *Journal of Climate*, *30*(24), 10019–10036. https://doi.org/10.1175/jcli-d-17-0300.1

Huang, H., Qian, Y., He, C., Bair, E. H., & Rittger, K. (2022). Snow albedo feedbacks enhance snow impurity-induced radiative forcing in the Sierra Nevada. *Geophysical Research Letters*, *49*(11), e2022GL098102. https://doi.org/10.1029/2022GL098102

Kaempfer, T. U., Hopkins, M. A., & Perovich, D. K. (2007). A three-dimensional microstructure-based photon-tracking model of radiative transfer in snow. *Journal of Geophysical Research*, *112*(D24). https://doi.org/10.1029/2006jd008239

Kokhanovsky, A. A., & Zege, E. P. (2004). Scattering optics of snow. *Applied Optics*, *43*(7), 1589–1602. https://doi.org/10.1364/ao.43.001589

Larue, F., Picard, G., Arnaud, L., Ollivier, I., Delcourt, C., Lamare, M., et al. (2020). Snow albedo sensitivity to macroscopic surface roughness using a new ray-tracing model. *The Cryosphere*, *14*(5), 1651–1672. https://doi.org/10.5194/tc-14-1651-2020

Lawrence, D. M., Fisher, R. A., Koven, C. D., Oleson, K. W., Swenson, S. C., Bonan, G., et al. (2019). The Community Land Model version 5: Description of new features, benchmarking, and impact of forcing uncertainty. *Journal of Advances in Modeling Earth Systems*, *11*(12), 4245–4287. https://doi.org/10.1029/2018MS001583

Lee, W. L., Liou, K. N., He, C., Liang, H. C., Wang, T. C., Li, Q., et al. (2017). Impact of absorbing aerosol deposition on snow albedo reduction over the southern Tibetan plateau based on satellite observations. *Theoretical and Applied Climatology*, *129*(3), 1373–1382. https://doi.org/10.1007/s00704-016-1860-4

Lei, Y., Pan, J., Xiong, C., Jiang, L., & Shi, J. (2023). Snow depth and snow cover over the Tibetan Plateau observed from space in against ERA5: Matters of scale. *Climate Dynamics*, *60*(5–6), 1523–1541. https://doi.org/10.1007/s00382-022-06376-0

Li, C., Yan, F., Kang, S., Yan, C., Hu, Z., Chen, P., et al. (2021). Carbonaceous matter in the atmosphere and glaciers of the Himalayas and the Tibetan plateau: An investigative review. *Environment International*, *146*, 106281. https://doi.org/10.1016/j.envint.2020.106281

Libois, Q., Picard, G., Dumont, M., Arnaud, L., Sergent, C., Pougatch, E., et al. (2014). Experimental determination of the absorption enhancement parameter of snow. *Journal of Glaciology*, *60*(222), 714–724. https://doi.org/10.3189/2014JoG14J015

Libois, Q., Picard, G., France, J. L., Arnaud, L., Dumont, M., Carmagnola, C. M., & King, M. D. (2013). Influence of grain shape on light penetration in snow. *The Cryosphere*, *7*(6), 1803–1818. https://doi.org/10.5194/tc-7-1803-2013

Liou, K. N., Takano, Y., He, C., Yang, P., Leung, L. R., Gu, Y., & Lee, W. L. (2014). Stochastic parameterization for light absorption by internally mixed BC/dust in snow grains for application to climate models. *Journal of Geophysical Research: Atmospheres*, *119*(12), 7616–7632. https://doi.org/10.1002/2014JD021665

Liu, D., He, C., Schwarz, J. P., & Wang, X. (2020). Lifecycle of light-absorbing carbonaceous aerosols in the atmosphere. *NPJ Climate and Atmospheric Science*, *3*(1), 40. https://doi.org/10.1038/s41612-020-00145-8

Malle, J., Rutter, N., Webster, C., Mazzotti, G., Wake, L., & Jonas, T. (2021). Effect of forest canopy structure on wintertime land surface albedo: Evaluating CLM5 simulations with in-situ measurements. *Journal of Geophysical Research: Atmospheres*, *126*(9), e2020JD034118. https://doi.org/10.1029/2020JD034118

Manninen, T., Anttila, K., Jääskeläinen, E., Riihelä, A., Peltoniemi, J., Räisänen, P., et al. (2021). Effect of small-scale snow surface roughness on snow albedo and reflectance. *The Cryosphere*, *15*(2), 793–820. https://doi.org/10.5194/tc-15-793-2021

Mortimer, C., Mudryk, L., Derksen, C., Luojus, K., Brown, R., Kelly, R., & Tedesco, M. (2020). Evaluation of long-term Northern Hemisphere snow water equivalent products. *The Cryosphere*, *14*(5), 1579–1594. https://doi.org/10.5194/tc-14-1579-2020

Muñoz Sabater, J. (2019). ERA5-Land monthly averaged data from 1950 to present [Dataset]. Copernicus Climate Change Service (C3S) Climate Data Store (CDS). https://doi.org/10.24381/cds.68d2bb30

Oaida, C. M., Xue, Y., Flanner, M. G., Skiles, S. M., De Sales, F., & Painter, T. H. (2015). Improving snow albedo processes in WRF/SSiB regional climate model to assess impact of dust and black carbon in snow on surface energy balance and hydrology over western US. *Journal of Geophysical Research: Atmospheres*, *120*(8), 3228–3248. https://doi.org/10.1002/2014jd022444

Painter, T. H., Deems, J. S., Belnap, J., Hamlet, A. F., Landry, C. C., & Udall, B. (2010). Response of Colorado River runoff to dust radiative forcing in snow. *Proceedings of the National Academy of Sciences of the United States of America*, *107*(40), 17125–17130. https://doi.org/10.1073/pnas.0913139107

Perovich, D. K., & Govoni, J. W. (1991). Absorption coefficients of ice from 250 to 400 nm. *Geophysical Research Letters*, *18*(7), 1233–1235. https://doi.org/10.1029/91GL01642

Picard, G., Dumont, M., Lamare, M., Tuzet, F., Larue, F., Pirazzini, R., & Arnaud, L. (2020). Spectral albedo measurements over snow-covered slopes: Theory and slope effect corrections. *The Cryosphere*, *14*(5), 1497–1517. https://doi.org/10.5194/tc-14-1497-2020

Picard, G., Libois, Q., & Arnaud, L. (2016). Refinement of the ice ab-sorption spectrum in the visible using radiance profile measurements in Antarctic snow. *The Cryosphere*, *10*(6), 2655–2672. https://doi.org/10.5194/tc-10-2655-2016

Polashenski, C. M., Dibb, J. E., Flanner, M. G., Chen, J. Y., Courville, Z. R., Lai, A. M., et al. (2015). Neither dust nor black carbon causing apparent albedo decline in Greenland's dry snow zone: Implications for MODIS C5 surface reflectance. *Geophysical Research Letters*, *42*(21), 9319–9327. https://doi.org/10.1002/2015GL065912

Pu, W., Shi, T., Cui, J., Chen, Y., Zhou, Y., & Wang, X. (2021). Enhancement of snow albedo reduction and radiative forcing due to coated black carbon in snow. *The Cryosphere*, *15*(5), 2255–2272. https://doi.org/10.5194/tc-15-2255-2021

Qian, Y., Yasunari, T. J., Doherty, S. J., Flanner, M. G., Lau, W. K., Ming, J., et al. (2015). Light-absorbing particles in snow and ice: Measurement and modeling of climatic and hydrological impact. *Advances in Atmospheric Sciences*, *32*(1), 64–91. https://doi.org/10.1007/s00376-014-0010-0

Räisänen, P., Makkonen, R., Kirkevåg, A., & Debernard, J. B. (2017). Effects of snow grain shape on climate simulations: Sensitivity tests with the Norwegian Earth system model. *The Cryosphere*, *11*(6), 2919–2942. https://doi.org/10.5194/tc-11-2919-2017

Robledano, A., Picard, G., Dumont, M., Flin, F., Arnaud, L., & Libois, Q. (2023). Unraveling the optical shape of snow. *Nature Communications*, *14*(1), 3955. https://doi.org/10.1038/s41467-023-39671-3

Roeckner, E., Bauml, G., Bonaventura, L., Brokopf, R., Esch, M., Giorgetta, M., et al. (2003). *The atmospheric general circulation model ECHAM5. Part I: Model description*. Rep 349 (p. 127). Max Planck Institute for Meteorology.

Saito, M., Yang, P., Loeb, N. G., & Kato, S. (2019). A novel parameterization of snow albedo based on a two-layer snow model with a mixture of grain habits. *Journal of the Atmospheric Sciences*, *76*(5), 1419–1436. https://doi.org/10.1175/jas-d-18-0308.1

Scanza, R. A., Mahowald, N., Ghan, S., Zender, C. S., Kok, J. F., Liu, X., et al. (2015). Modeling dust as component minerals in the community atmosphere model: Development of framework and impact on radiative forcing. *Atmospheric Chemistry and Physics*, *15*(1), 537–561. https://doi.org/10.5194/acp-15-537-2015

Schaaf, C., & Wang, Z. (2021). MODIS/Terra+Aqua BRDF/Albedo Albedo Daily L3 Global 0.05Deg CMG V061 [Dataset]. NASA EOSDIS Land Processes DAAC. https://doi.org/10.5067/MODIS/MCD43C3.061

Shi, T., Cui, J., Chen, Y., Zhou, Y., Pu, W., Xu, X., et al. (2021). Enhanced light absorption and reduced snow albedo due to internally mixed mineral dust in grains of snow. *Atmospheric Chemistry and Physics*, *21*(8), 6035–6051. https://doi.org/10.5194/acp-21-6035-2021

Shi, T., He, C., Zhang, D., Zhang, X., Niu, X., Xing, Y., et al. (2022). Opposite effects of mineral dust nonsphericity and size on dust-induced snow albedo reduction. *Geophysical Research Letters*, *49*(12), e2022GL099031. https://doi.org/10.1029/2022gl099031

Skiles, S. M., Flanner, M., Cook, J. M., Dumont, M., & Painter, T. H. (2018). Radiative forcing by light-absorbing particles in snow. *Nature Climate Change*, *8*(11), 964–971. https://doi.org/10.1038/s41558-018-0296-5

Skiles, S. M., & Painter, T. (2017). Daily evolution in dust and black carbon content, snow grain size, and snow albedo during snowmelt, Rocky Mountains, Colorado. *Journal of Glaciology*, *63*(237), 118–132. https://doi.org/10.1017/jog.2016.125

Stamnes, K., Tsay, S. C., Wiscombe, W., & Jayaweera, K. (1988). Numerically stable algorithm for discrete-ordinate-method radiative transfer in multiple scattering and emitting layered media. *Applied Optics*, *27*(12), 2502–2509. https://doi.org/10.1364/ao.27.002502

Thackeray, C. W., & Fletcher, C. G. (2016). Snow albedo feedback: Current knowledge, importance, outstanding issues and future directions. *Progress in Physical Geography*, *40*(3), 392–408. https://doi.org/10.1177/0309133315620999

Thackeray, C. W., Fletcher, C. G., & Derksen, C. (2019). Diagnosing the impacts of Northern Hemisphere surface albedo biases on simulated climate. *Journal of Climate*, *32*(6), 1777–1795. https://doi.org/10.1175/jcli-d-18-0083.1

Toon, O. B., McKay, C. P., Ackerman, T. P., & Santhanam, K. (1989). Rapid calculation of radiative heating rates and photodissocia-tion rates in inhomogeneous multiple scattering atmospheres. *Journal of Geophysical Research*, *94*(D13), 16287–16301. https://doi.org/10.1029/jd094id13p16287

Toure, A. M., Luojus, K., Rodell, M., Beaudoing, H., & Getirana, A. (2018). Evaluation of simulated snow and snowmelt timing in the Community Land Model using satellite-based products and streamflow observations. *Journal of Advances in Modeling Earth Systems*, *10*(11), 2933–2951. https://doi.org/10.1029/2018MS001389

Tuzet, F., Dumont, M., Lafaysse, M., Picard, G., Arnaud, L., Voisin, D., et al. (2017). A multilayer physically based snowpack model simulating direct and indirect radiative impacts of light-absorbing impurities in snow. *The Cryosphere*, *11*(6), 2633–2653. https://doi.org/10.5194/tc-11-2633-2017

Verseghy, D. L. (1991). CLASS–A Canadian land surface scheme for GCMs. I. Soil model. *International Journal of Climatology*, *11*(2), 111–133. https://doi.org/10.1002/joc.3370110202

Vionnet, V., Brun, E., Morin, S., Boone, A., Faroux, S., Le Moigne, P., et al. (2012). The detailed snowpack scheme Crocus and its implementation in SURFEX v7. 2. *Geoscientific Model Development*, *5*(3), 773–791. https://doi.org/10.5194/gmd-5-773-2012

Wang, W., He, C., Moore, J., Wang, G., & Niu, G. Y. (2022). Physics-based narrowband optical parameters for snow albedo simulation in climate models. *Journal of Advances in Modeling Earth Systems*, *14*(1), e2020MS002431. https://doi.org/10.1029/2020ms002431

Warren, S. G. (1984). Optical constants of ice from the ultraviolet to the microwave. *Applied Optics*, *23*(8), 1206–1225. https://doi.org/10.1364/ao.23.001206

Warren, S. G., & Brandt, R. E. (2008). Optical constants of ice from the ultraviolet to the microwave: A revised compilation. *Journal of Geophysical Research*, *113*(D14), D14220. https://doi.org/10.1029/2007JD009744

Warren, S. G., & Wiscombe, W. J. (1980). A model for the spectral albedo of snow. II: Snow containing atmospheric aerosols. *Journal of the Atmospheric Sciences*, *37*(12), 2734–2745. https://doi.org/10.1175/1520-0469(1980)037<2734:amftsa>2.0.co;2

Williamson, C. J., Cook, J., Tedstone, A., Yallop, M., McCutcheon, J., Poniecka, E., et al. (2020). Algal photophysiology drives darkening and melt of the Greenland Ice Sheet. *Proceedings of the National Academy of Sciences of the United States of America*, *117*(11), 5694–5705. https://doi.org/10.1073/pnas.1918412117

Wiscombe, W. J., & Warren, S. G. (1980). A model for the spectral albedo of snow. I: Pure snow. *Journal of the Atmospheric Sciences*, *37*(12), 2712–2733. https://doi.org/10.1175/1520-0469(1980)037<2712:amftsa>2.0.co;2

Yan, F., He, C., Kang, S., Chen, P., Hu, Z., Han, X., et al. (2019). Deposition of organic and black carbon: Direct measurements at three remote stations in the Himalayas and Tibetan Plateau. *Journal of Geophysical Research: Atmospheres*, *124*(16), 9702–9715. https://doi.org/10.1029/2019jd031018

Yang, Z. L., Dickinson, R. E., Robock, A., & Vinnikov, K. Y. (1997). Validation of the snow submodel of the biosphere–atmosphere transfer scheme with Russian snow cover and meteorological observational data. *Journal of Climate*, *10*(2), 353–373. https://doi.org/10.1175/1520-0442(1997)010<0353:votsso>2.0.co;2

Yi, K., Meng, J., Yang, H., He, C., Henze, D. K., Liu, J., et al. (2019). The cascade of global trade to large climate forcing over the Tibetan Plateau glaciers. *Nature Communications*, *10*(1), 1–9. https://doi.org/10.1038/s41467-019-10876-9

Young, C. L., Sokolik, I. N., Flanner, M. G., & Dufek, J. (2014). Surface radiative impacts of ash deposits from the 2009 eruption of Redoubt volcano. *Journal of Geophysical Research: Atmospheres*, *119*(19), 11–387. https://doi.org/10.1002/2014jd021949